SCIEPublish

Review

Mechanistic Insights into Photocatalytic WO_3 for Hydrogen Generation

Preetha Chandrasekharan Meenu, Bhagatram Meena and Panagiotis G. Smirniotis *

Department of Chemical and Environmental Engineering, University of Cincinnati, Cincinnati, OH 45221, USA; meenupc06@gmail.com (P.C.M.); bhagatrammeena1010@gmail.com (B.M.)

* Corresponding author. E-mail: smirnipp@ucmail.uc.edu (P.G.S.)

Received: 12 January 2025; Accepted: 11 March 2025; Available online: 14 March 2025

ABSTRACT: Growing environmental concerns and the limitations of fossil fuel resources have recently led to increased focus on clean and renewable energy sources. Hydrogen (H_2) has gained importance as an alternative clean fuel with its potential to become the primary chemical energy carrier. Photocatalytic hydrogen generation offers a capable solution to the energy crisis and has gained significant attention as a renewable energy solution, offering independence from fossil fuels and zero carbon dioxide emissions. Tungsten oxide (WO_3) offers to be a promising photocatalyst for Hydrogen Evolution Reaction (HER) with its ability to tune the band gap, robust absorption in the visible spectrum range, steadiness in harsh reaction conditions, low cost, and reduced toxicity. Various synthetic methods can be employed to fabricate photocatalysts with diverse morphologies, sizes, and structures, all of which significantly influence their catalytic performance to varying extents. This review goals to explicitly highlight and discourse the main properties of WO_3 and its modifications for photocatalytic HER via different synthesis methods. Modification in WO_3 to its corresponding composites, heterojunctions are explicitly explained in this review.

Keywords: Photocatalysts; HER; WO_3; Band gap; Quantum yield; Composites

1. Introduction

Urbanization and industrialization form the foundation of modern civilization, driving substantial economic growth, technological advancements, and enhanced living standards. These processes have contributed to the rising universal energy demand through sustainable and environmentally friendly solutions which is a key challenge of the 21st century. The primary energy source has been covered by fossil fuels for industry and transportation which is being severely depleted at a rapid rate. Fossil fuels combustion significantly contributes to environmental issues through the generation and release of harmful by-product gases such as NO_X, SO_2, and CO_2. Among these, CO_2 is a major pollutant, not only from fossil fuel combustion but also from various other human activities. Its accumulation intensifies the greenhouse effect, ultimately driving global warming [1,2]. Therefore, addressing the reduction of these toxic gases is crucial. Clean energy systems are essential for minimizing reliance on fossil fuels and reducing environmental harm.

In recent times, researchers have become increasingly attentive to achieving environmental sustainability and tackling the growing crisis of environmental pollution. Hydrogen (H_2) stands out in the energy market for the upcoming decades with numerous benefits when considered with other traditional fuels such as petroleum and coal [3–5]. Its ability to be stored for extended periods and transported across locations makes it a promising solution for upcoming needs for energy. In the long run, hydrogen fuel will replace hydrocarbon fuels because of its benefits and adaptability. Even though hydrogen is considered to be a potential candidate, its generation from hydrocarbons, is required for a low greenhouse gas (GHG) scenario. Solar, a zero carbon but renewable source of energy can fulfil the energy requirement of the world by its proper implementation. Hydrogen production photo catalytically is attracting significant attention as a promising self-determining method for efficient energy generation as it relies on water and sunlight—resources that are abundant and virtually limitless [6–9]. This approach is effective as it addresses energy demands as well as reduces the reliance towards fossil fuels. The idea of Honda and Fujishima of photo assisted hydrogen and oxygen generation

https://doi.org/10.70322/prp.2025.10007

by water splitting in 1972 paved the way for various approaches and photocatalysts for solar light driven catalytic H_2 production [10]. Despite its potential, the progress of hydrogen production via photocatalysis has been slower as it faces a myriad of challenges. The primary challenge lies in its low efficiency, catalyst long term activity, band gap engineering, and reactor design that are largely influenced by the quantum efficiency [11,12]. These challenges demand the need for innovative and strategic solutions to make hydrogen as a clean energy source solutions to make it realistic for the future generation.

Over four decades of research, some hundreds of photocatalysts have been explored in the area of oxides [13,14], alloys [15,16], metal free catalysts [7,17], Metal Organic Frameworks (MOF) [18,19], organic polymers and complexes. TiO_2 has been the most widely considered and established since the early 20th century, owing to its non-toxicity, wide availability, stability, and affordability [10,20,21]. The efficiency of TiO_2 remains significantly below the desired level due to several limitations, including its inability to utilize visible light effectively, a wide band gap (3.2 eV) resulting in low efficiency in the visible spectrum, slow mobility and kinetics of photogenerated charges, and rapid combination of generated electrons and holes. An ideal photocatalyst should have a band gap smaller than 3.0 eV to effectively capture and utilize visible light. To address these challenges, various innovative approaches, such as morphology engineering [22–24], elemental doping [25–28], heterojunction formation [29–31] *etc.*, have been investigated to enrich TiO_2 performance in various photocatalytic applications. Still tremendous investigations are going on band gap modification, stability and other properties of semiconductor based photocatalysts. Some of these semiconductors include g-C_3N_4 [32,33], $KTaO_3$ [34,35], ZrO_2 [36,37], $SrTiO_3$ [38,39] TiO_2 [20,40] and $BiVO_4$ [41,42] *etc*. and the further modifications on these include the heterojunction formation, composites, elemental doping for enhanced photocatalytic HER.

WO_3 stands out as the most significant photocatalyst among metal oxides for the visible light region, owing to its remarkable chemical and physical properties. WO_3 is a promising semiconductor with comparatively lesser band gap energy of 2.8 eV along with the absorption capability in the visible spectrum [43–45]. Moreover, WO_3 is cost-effective, exhibits low toxicity, and undergoes structural rearrangements that result in various polymorphs (e.g., triclinic, monoclinic, orthorhombic, tetragonal, cubic, and hexagonal). It also possesses a high oxidizing ability of the valence band holes, stable physicochemical properties, excellent solar light responsiveness, and highly tuneable structures. These properties make WO_3 an outstanding catalyst for photocatalytic HER [46,47].

WO_3 is a capable photocatalyst for HER because of its capability to absorb visible light and its high stability harsh reaction conditions. The VB edge of WO_3 is around 2.8 eV (*vs.* NHE), making it suitable for water oxidation. However, the CB is not shifted to negative edge to ease water reduction. When WO_3 (p-type) is considered as photoanode, water reduction potential tends to be in the positive potential of CB. Consequently, in photoelectrochemical devices utilizing Pt is used as cathode and WO_3 as anode. This promotes WO_3 capability for OER in a photocatalytic system. One such example is where WO_3 with Pt was used for O_2 evolution and TaON with Pt acted as photocathode for HER in the photoelectrochemical system. The authors used IO^{3-}/I^- shuttle redox system to enhance oxygen generation [48].

Numerous studies have highlighted photocatalytic WO_3 and the optimization of their physicochemical properties for photocatalytic applications. Considering the plethora of studies conducted on WO_3 towards photocatalysis, this review work aims to highlight the properties, latest approachs and modifications in WO_3 based photocatalysts for HER. It also discusses the fundamental aspects of photocatalytic HER and evaluates the performance of photocatalysts in HER. Furthermore, this review provides a detailed overview of the latest synthesis methods and strategies designed to improve the photocatalytic efficiency of WO_3 for HER applications.

2. Minutes of Photocatalytic HER and Related Factors

Succinctly, photocatalytic HER is typically an uphill reaction that involves illuminating a semiconductor catalytic material with light, causing electrons in the VB to absorb energy and transition to the CB, creating holes in CB. This is the preliminary step, which is devoted to semiconductor's photoexcited state. The first prerequisite is the realisation of high solar to hydrogen ratio (STH) under solar irradiation and a photocatalyst with an appropriate band gap [3,49,50]. The excitation step is primarily determined by the electronic band structure of the catalyst and levels of the conduction and valence bands. A photocatalyst with a narrow bandgap, the smaller the light energy and longer the corresponding wavelength of light can produce a greater number of excited electrons–hole pairs under such identical illumination conditions. Additionally, the lowest energy level of the CB must be more negative than the redox potential of H^+/H_2 (0 V *vs.* NHE), whereas the highest energy level of the VB must be more positive than the redox potential of O_2/H_2O (1.23 V). In the subsequent phase, photogenerated carriers travel to the semiconductor's surface. Crystal structure,

crystallinity and particle size have significant impact on this stage leading to more effective hydrogen production [51,52]. Additionally, particle size reduction shortens the migration distance for photogenerated electrons and holes to reach surface reaction sites, which in turn reduces the likelihood of the rate of recombination [53]. The final phase involves the catalytic reaction on the surface, wherein the electrons and holes that have migrated to the catalyst's surface react with the adsorbed substrate. The photogenerated electrons decrease H^+ to produce H_2, whereas the photogenerated holes oxidize H_2O to make oxygen, as illustrated in Figure 1.

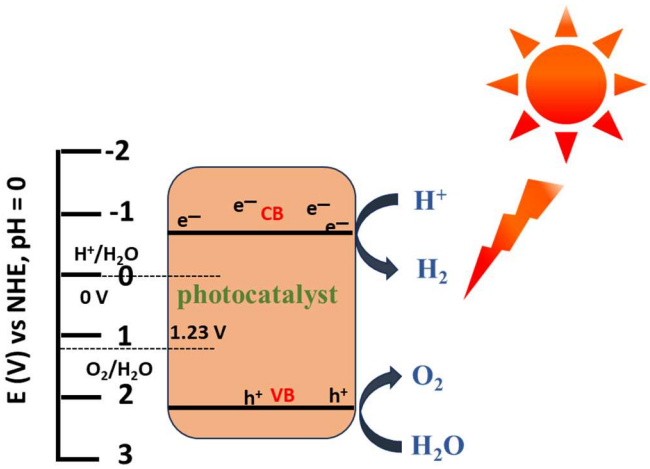

Figure 1. Schematic representation of photocatalytic water splitting.

Surface area and active sites are the main criteria of this step [8,49,54–56].

The general mechanism of photocatalytic HER is shown in equation below:

$$\text{Photocatalysts} \xrightarrow{h\gamma} h^+ + e^-$$

$$4h^+ + 2H_2O \rightarrow O_2 + H_4^+$$

$$4H^+ + 4e^- \rightarrow 2H_2$$

All the abovementioned steps mark H_2 generation from the semiconductor photocatalysts. Once electron/hole pairs are made, charge separation and recombination are two competitive steps that happen inside the semiconductor photocatalyst. These play a part in how well photocatalytic water splitting works to make hydrogen. Charge recombination is a thermodynamically favourable process that happens almost instantaneously either on the surface or in bulk. This phenomenon is regarded as a deactivation process and renders water splitting ineffective [11,56]. Another critical challenge to address is the surface back reaction, where H_2O is formed on the surface of the photocatalyst from the generated H_2 and O_2 [57,58]. In recent years, significant advancements have been achieved to overcome these obstacles, focusing on catalyst design, reactor engineering, and the use of sacrificial agents, co-catalysts, and other innovative strategies.

2.1. Assessment of Photocatalytic Water Splitting

A collection of crucial metrics that are often used to quantitatively describe the substrate conversion efficiency is used to assess the rate of H_2 evolution during photocatalytic HER. This efficiency is described by the concept of overall quantum yield [59,60]. Under the given irradiation circumstances, the rate of gas evolution is typically measured as mol/h per catalyst quantity [g]. The overall quantum yield for H_2 generation is calculated using the following equation:

$$\text{Quantum yield (\%)} = \left(\frac{2 \times \text{Number of evolved } H_2 \text{ molecules}}{\text{Number of incident photons}} \times 100\right)$$

Quantum yield is precise in homogeneous processes. In heterogeneous systems, it provides an estimate of the amount of incident photons on the surface of the catalyst, which represents the maximum number of photons that could be absorbed. As a result, the idea of photonic yield has been introduced. It represents the photoreaction rate observed over a specific time period to the rate of photons incident within a particular wavelength range passing through the irradiation window of the reactor [61,62].

The second parameter for the assessment of H_2 evolution photo catalytically is Turnover number (TON). TON is often defined as the ratio of reacting molecules to active sites. TON is given by the equation:

$$\text{TON} = \frac{\text{Number of molecules reacted}}{\text{Number of active sites}}$$

The determination of photocatalyst active sites is indigenous. Thus, TON can be expressed as the proportion of reacting electrons to atoms in a photocatalyst.

$$\text{TON} = \frac{\text{Number of reacted electrons}}{\text{Number of atoms at the surface of photocatalyst}}$$

Even though all these parameters are considered, it is necessary to keep in mind some crucial points while evaluating the quantum yield.

(i) Optimize the quantity of photocatalyst for each experimental setup, ensuring it does not alter the reaction rate. In addition, the catalyst should be dispersed evenly, which can be accomplished through effective stirring.
(ii) Consider initial reactant consumption and product production rates to avoid interference with measurements and reduce catalyst deactivation. Particularly, the quantum yield for substrate utilization and product production frequently fluctuates with irradiation time, especially during prolonged exposure.
(iii) Before light irradiation, reactants adsorbed on catalysts should reach a stable state, and the reaction rate should be proportional to the irradiation.

2.2. Factors Affecting Efficiency of Photocatalysts

2.2.1. Band Gap

One important thing that affects how well HER works is the band gap of a photocatalyst. Light harvesting, the efficient separation, transfer of photogenerated charge carriers, and surface reactions are the only things that make photocatalytic HER work. The semiconductor's band gap must cover the reduction and oxidation potentials of water, which are +0 V and +1.23 V *vs.* NHE, respectively, when the source solution has a pH of 0. According to theory, a semiconductor's VB should be less than the redox potential of O_2/H_2O and its CB should be more than the redox potential of H^+/H_2. Thermodynamically, the initial step is the hydrogenation of intermediates; the active site absorbs H^+ to reduce to H_2 by use of photoelectrons. Even though there are numerous stable photocatalysts developed, the main constrain that prevails is the wide band gap, which hinders overall photocatalytic efficiency. Many researchers have concentrated on creating visible-light-responsive photocatalysts that are stable and have adequate band gap. Even the most effective and widely used photocatalyst TiO_2 faces limitations in meeting the requisite property of a photocatalyst, which has a band gap of 3.2 eV [63]. In such scenario, creating bandgap tuneable semiconductors is especially useful, which is considered to be a more promising approach to solar H_2 production than the single photocatalyst-based water splitting system. Heteroatom doping and the utilization of material junctions are two well-known techniques for changing photocatalyst bandgaps and band locations. One of the best ways to make photocatalysts work better was to coat them with noble metal. This is because the noble metal particles on the surface of the TiO_2 can act as electron sinks, storing and moving photogenerated electrons. This helps separate charge carriers and lowers the rate at which they recombine. Some of the noble metals adopted include Pt [64,65], Ru [66,67] and Pd [68,69], *etc.* Owing to the expensive part of noble metals, the other strategies adopted for the tunning of the band gap are the generation of composite photocatalysts of non-noble metals over singular ones [70,71], doping with metals and non-metals [72], creating anion [73,74], and cation [75] vacancies. These variations have a substantial impact on the band structure of semiconductors by changing how materials react to visible light, creating new energy levels across the band structures of the host semiconductor, increasing light absorption, allowing low-energy excitations, charge separation, and speeding up the separation of charges and catalytic activity for photocatalytic HER.

2.2.2. pH and Temperature

The pH of a solution is a crucial component in photocatalytic processes, as it significantly influences the process by affecting the adsorption of substrates onto the photocatalyst surface. It is very important that the pH of the photocatalytic system changes because it affects where the VB and CB edges are located. This, in turn, affects the semiconductor's ability to oxidize or reduce, as shown in the equation below:

$$E_{vb} = E_{vb}^{0} - 0.059\text{pH}$$

$$E_{cb} = E_{cb}^{0} - 0.059\text{pH}$$

where E_{vb}^{0} and E_{cb}^{0} are the VB and CB potentials at zero pH. Estahbanati et al. looked at how pH affects the rates of photocatalytic HER in great detail [76]. They looked at different alcohols, such as ethanol, glycerol, and methanol, at pH levels ranging from 2 to 12. Using Pt/TiO_2 as the photocatalyst, they saw that the production of hydrogen peaked at a pH of about 8 for all substrates. This was because the catalyst clumped together and the TiOH groups broke apart, as seen in Figure 2. Another study examined the impact of pH variations on the photocatalytic HER mechanism, focusing on the role of dissolved metal ions as electron scavengers (metal ions) and hole scavenger (methanol). This study found significant changes in VB and CB edges by pH variations throughout photocatalytic water splitting over WO_3, TiO_2 (rutile), and NiO employing a 355 nm laser source [77].

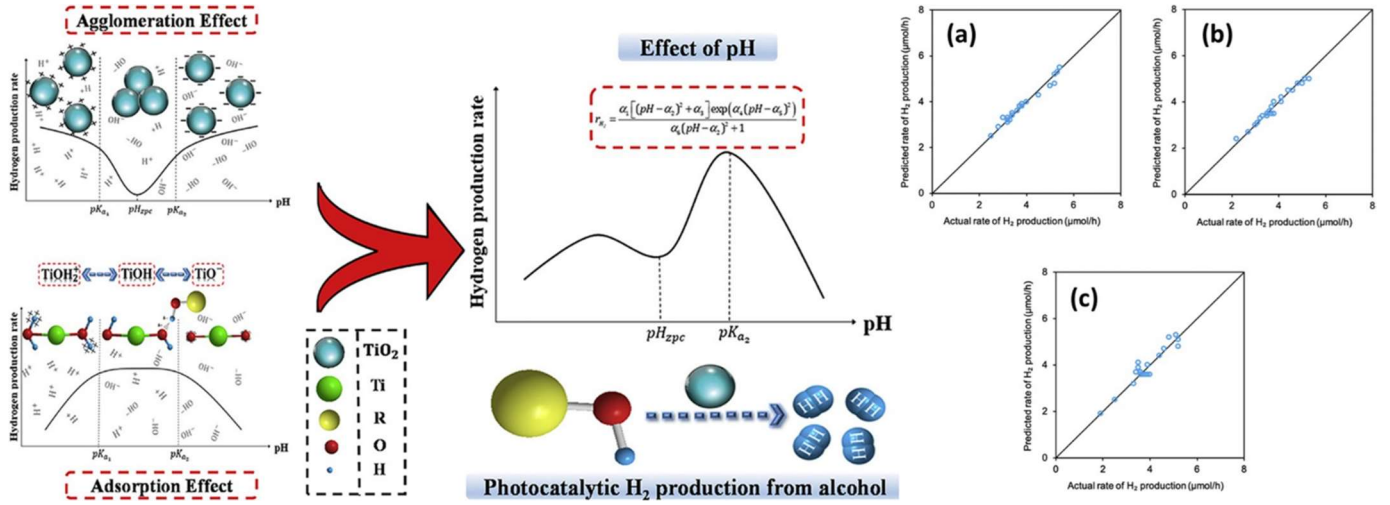

Figure 2. Kinetics on photocatalytic HER on Pt/TiO_2 on different alcohols. The rate of hydrogen production based on the present experimental results for glycerol (**a**), ethanol (**b**), and methanol (**c**) [76]. Copyright 2019, Elsevier.

The production of electron-hole pairs is not directly influenced by temperature, which is why it has an insignificant impact on photocatalytic activity. However, temperature shows a substantial influence on the desorption of reaction products from the catalyst surface, accelerating the overall reaction rate. The temperature effect on photocatalysis differs depending on the photocatalyst. At higher temperatures, the possibility of transfer of electrons from the VB to higher energy states increases, boosting the production of electron-hole pairs and aiding in the first oxidation and reduction processes. Lower temperatures, on the other hand, have a detrimental effect on the reaction rate because they decrease product desorption, limit reactant adsorption and reduce HER efficiency. Huaxu et al. analysed photocatalyst Pt/TiO_2 where it generated 4.71 mmol g^{-1} of H_2 in 4 h in 45 °C [78]. The hydrogen production increased to 15.18 mmol g^{-1} at 55 °C.

2.2.3. Light Intensity

Light intensity has the capability to enhance the photocatalytic water splitting that enhances energies above the activation threshold. Typically, a light source has the capacity to accelerate the formation of electron-hole pairs through chemical reactions rather than recombination reactions. Baniasadi et al. (2013) showed that using ZnS for photocatalytic hydrogen generation led to a 20% rise in photoactivity when light strength was raised from 900 to 1000 W m^{-2} [79].

2.2.4. Sacrificial Agents

Sacrifice agents are catalysts that play a prominent role in photocatalytic H_2 production by diminishing the recombination of e^{-}-h^{+} recombination and holes to enhance photocatalytic hydrogen generation. Electron donors are used as sacrificial agents and scavenge the holes reducing charge carrier recombination. Further, the back reaction of the formation of water is suppressed, increasing the H_2 yield. The water-splitting reaction with the presence of sacrificial agents is a less uphill reaction than without sacrificial agents. The most common sacrificial agents include triethanolamine, sodium sulfide/sodium sulfite and methanol [80]. The selection and concentration of sacrificial agents play a drastic role in photocatalytic hydrogen generation. For example, Na_2S/Na_2SO_3 mixture, methanol and

triethanolamine (TEOA) are the most suitable sacrificial agents for sulphides, oxides and carbon based photocatalysts, respectively. TEOA can, for example, take in photogenerated holes and strengthen the bond between carbon-based g-C_3N_4 and H_2O, which speeds up the splitting and movement of photogenerated carriers on the surface [81]. Among alcohols, methanol is considered to be the ideal sacrificial agent with one hydroxyl group and was the ideal feedstock for photo reforming reactions. This is attributed to the fast h^+ transfer process. The addition of methanol donates electrons that react irreversibly with photogenerated VB and enhances e^--h^+ efficiency resulting in higher quantum efficiency. Bowker et al. demonstrated that applying primary alcohols over Au/TiO_2 catalysts resulted in higher rates of H_2 generation, whereas tertiary alcohols exhibited only minimal activity [82]. Na_2S/Na_2SO_3 mixture acts as sacrificial inorganic since it is a particularly efficient hole acceptor, allowing for successful charge carrier separation. Na_2S/Na_2SO_3 mixture has been mostly used in sulphide-based catalysts such as CdS due to its more oxidisable nature compared to alcohol and reducing the undesired photocorrosion. Also, if there is sulfide in the solution around the Cd^{2+}, it can mix with S^{2-} to make CdS again [83].

3. Main Properties of WO_3

The crystal phases of WO_3 semiconductor (n-type) change over the temperature range of −180 °C to 900 °C. At temperatures ranging from 17 to 330 °C, the monoclinic I phase (γ-WO_3) develops, whereas the monoclinic II phase (ε-WO_3) is seen above − 43 °C. Between − 43 and 17 °C, the triclinic phase (δ-WO_3) takes place, and between 330 and 740 °C, the orthorhombic beta phase (β-WO_3) appears. At temperatures exceeding 740 °C, the tetragonal phase (α-WO_3) is formed as shown in Figure 3. The most stable of these phases is γ-WO_3, which has a monoclinic crystal structure and a band gap energy between 2.4 and 2.8 eV. It is also the form of WO_3 that has been studied the most [84–86]. Monoclinic WO_3 features a perovskite-like structure with a space group of P21/n, comprising a network of WO_6 octahedra. Each WO_6 unit is composed of eight tungsten atoms and 24 oxygen atoms, with edges shared by 8 oxygen atoms. These octahedra form a slightly distorted cubic arrangement within the structure. This well-defined atomic arrangement and high structural controllability create favourable conditions for achieving efficient photocatalytic activity. Also, the holes on the VB of WO_3 have a high oxidation potential (>2.5 eV), which means they can change OH^- into a hydroxyl radical. This makes it suitable for photocatalytic oxidation reactions, especially in the removal of environmental pollutants. Further, WO_3 is widely used in areas including photocatalytic disinfection, gas sensing, hydrogen evolution reactions, organic contaminant degradation in water by photocatalysis and photoelectrocatalysis and energy storage.

The deep valence band position of WO_3 of about 3.4 V makes it an efficient catalyst for visible light induced O_2 evolution. Considering its efficiency in photocatalytic OER, various strategies can be adopted to enhance its photocatalytic HER. This includes template-based synthesis, nano structuring, metal and non-metal doping, phase engineering, heterojunction formation *etc.* One strategy adopted is enhancing the oxygen vacancy of WO_3 resulting in increased HER activity relative to their pristine WO_3 [87]. The others include enhancing the surface properties and band gap via doping, defect engineering, pairing WO_3 with hydrogen evolution photocatalysts in a Z-scheme system that can leverage its strong oxidation ability while enhancing overall charge carrier separation.

The modification in WO_3 which includes morphology, size, crystal defects and exposed faces via different synthesis techniques can tune its optical and electrical properties. Nevertheless, the quick recombination of electrons and holes in WO_3, similar to other metal oxides, impedes its photocatalytic activity, resulting in a further decline in efficiency. Various methods are adopted to overcome this limitation, which include morphology engineering, crystal facet optimization, engineering of defects based on vacant oxygen, metal doping, creation of composites with carbon, heterojunction construction using a different semiconductor, and so on.

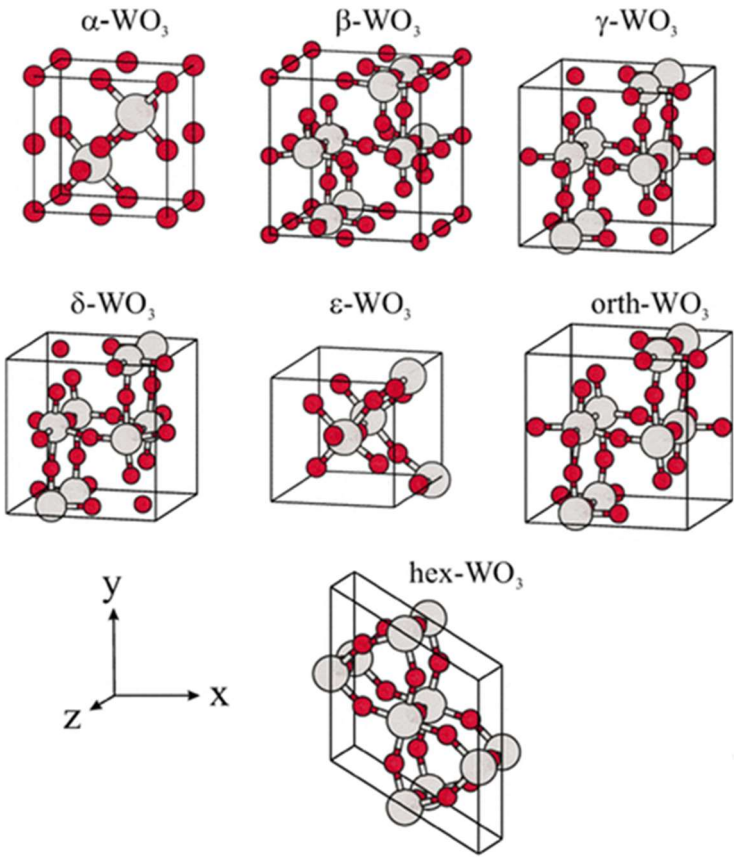

Figure 3. Phases of WO_3 (tungsten—grey balls and oxygen—red balls) [84]. Copyright 2022, Elsevier.

3.1. Synthesis Strategies of WO_3

Synthesis strategies play an important part in tunning and optimising the parameters of WO_3 based photocatalysts for better efficacy towards HER. Basically, the synthesis technique utilized to produce metal oxide, whether in film or powder form, should be simple, cost effective, easy to handle, and capable of mass production of the product. Different synthesis strategies can be adopted to modify the structure, shape, properties and size of WO_3 which to a large extent can affect the photocatalytic activity. Different synthetic strategies have been reported which are environmentally friendly and less expensive, but at the same time have amazing photocatalytic properties. The predominant synthesis methods employed include sol-gel, hydrothermal, co-precipitation, solution combustion, *etc*.

3.1.1. Co-Precipitation Method (CPM)

The coprecipitation approach is quick and economical for synthesizing metal oxides, involving the simultaneous formation of oxide particles during the precipitation process. This method integrates nucleation, growth, coarsening, and aggregation, offering key advantages such as homogeneity, precise composition control, and low-temperature synthesis compared to traditional techniques [88]. Additionally, it requires neither expensive equipment nor stringent reaction conditions, rendering it a cost-efficient and straightforward approach. This method is widely employed for the development of double hydroxides and can be optimized by adjusting the pH, which significantly influences the structure, size, and activity of the synthesized materials. Numerous researchers have utilized the coprecipitation method for synthesizing WO_3 and its composites to enhance photocatalytic performance. For instance, a study on $WO_3/CoWO_4$ nanocomposites with varying cobalt concentrations (5–20 wt%) demonstrated improved photocatalytic efficiency, with 20 wt% Co@WO_3 showing the best performance. The coprecipitation process produced catalysts with smaller crystalline sizes, lowered band gap of 2.51 eV and larger surface areas, which contributed to their effectiveness in degrading harmful contaminants in water. Degradation efficiency of 86.50% was exhibited by 20 wt% Co@WO_3 towards methylene blue [89]. Research by Banic et al. on novel WO_3/Fe_3O_4 magnetic photocatalysts was synthesised by the co-precipitation method using sodium tungstate and Na_2SO_4 precursors. During the synthesis by co-precipitation at pH of 1.8 WO_3 exhibited hexagonal morphology, while at pH 0.4 monoclinic morphology was adopted. This can be

ascribed to the rising WO_3 content, which enhances all textural parameters while maintaining its mesoporous characteristics, alongside the presence of hematite and magnetite Fe_3O_4 in the photocatalyst, as indicated by the XRD studies. The presence of WO_3 in magnetite enhanced the BET surface area. The researchers generated WO_3/Fe_3O_4 with varied amounts of WO_3, and 6.1 $WO_3/Fe_3O_4/H_2O_2$ exhibited a degradation efficiency for thiacloprid that was 2.2 times more than that of bare Fe_3O_4, as illustrated in Figure 4 [90]. Another group attempted to explore the optical characteristics of Cu doped WO_3 nanoparticles using the straightforward CPM [91]. The nucleation process initiates in the Na_2WO_4 precursor, succeeded by the polymerization, culminating in a unique structural molecule. The optimum temperature (100 °C) eliminates the undesirable solvents, yielding a pure chemical. The process for doping Cu was also the same. The CPM offers numerous advantages, including high yield, low temperature *etc.* CPM yielded a monoclinic structure with space group P21/n with a morphology characterized by nano-plates and rods. The optical absorbance edge was detected between 350 and 500 nm, and the band gap energy values for bare and Cu doped WO_3 were 3.12 and 3.36 eV, respectively, using the Kubelka-Munk equation.

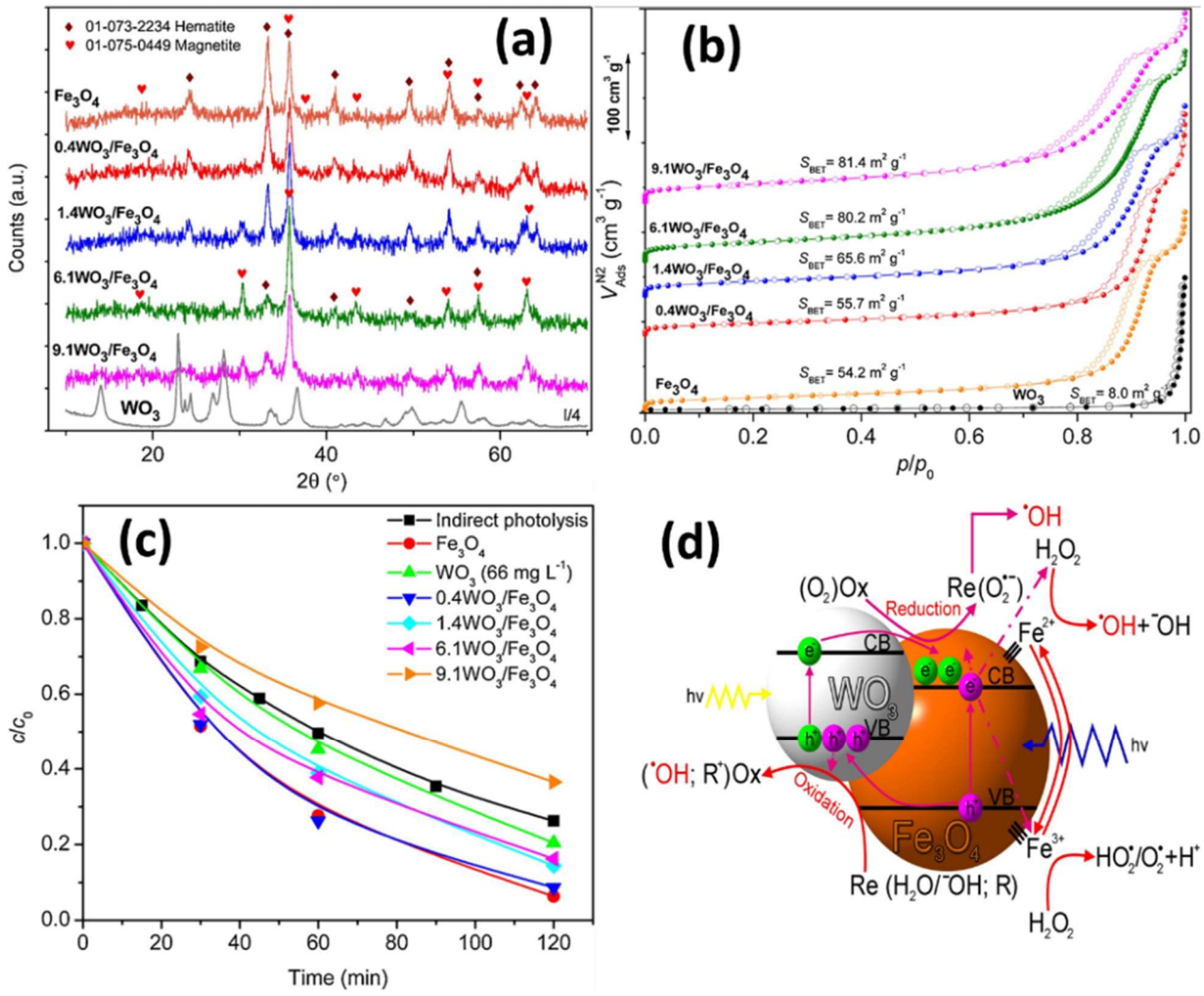

Figure 4. (**a**) XRD pattern of synthesised catalysts (**b**) BET of synthesised samples −196 °C (**c**) Kinetics of TCL photodegradation in WO_3/Fe_3O_4 in the presence of SS radiation (**d**) Charge transfer process [90]. Copyright 2019, Elsevier.

3.1.2. Hydrothermal Synthesis

The hydrothermal method is a useful solution-based approach for manufacturing metal oxides, conducted under conditions of elevated temperature and pressure. One of its key advantages is the ability to tailor the size, crystallinity, specific surface area and morphology by adjusting the reaction parameters, which significantly influences their photocatalytic activity. In hydrothermal synthesis, the compositions of oxides that are synthesized can be carefully controlled by using liquid phase or multiphase chemical processes. The hydrothermal method offers certain benefits including environmental friendliness, moderate conditions for operation, cheap prices, excellent dispersion in solution, production viability, less expensive instrumentation, and rapid synthesis. Hu et al. employed a straightforward

hydrothermal technique to synthesize one-dimensional hexagonally organized WO_3 nanorods with varied configurations. They used $SnCl_4 \cdot 5H_2O$ as the capping agent to improve photocatalytic activity [92]. Palharim et al. explored the variation of hydrothermal temperature in the shape of WO_3-AgCl composites. At a reaction temperature of 120 °C, WO_3 formed as agglomerated nanorods [93]. The shape of the WO_3 changed to agglomerated rectangular prisms at 180 °C. These may have fully surrounded the AgCl particles. Longer time results in thinner WO_3 nanorods at 120 °C and thicker prisms in rectangular shape at 180 °C. Growth of AgCl was more noticeable at 120 °C, particularly during the initial 12 h. The morphology of the catalysts, which was substantially influenced by both the reaction temperature and the synthesis duration, had a significant impact on the photocatalytic efficiency of the materials. Hexagonal WO_3 nanorods photocatalysts have been prepared through one-pot hydrothermal method using sodium tungstate in DI water as precursor by Yao et al. Nanorods exhibited BET surface area of 59.7 m^2g^{-1} and pore size distribution peak centres at about 6.12 nm. These nanorods demonstrated excellent photocatalytic activity for the breakdown of organic dyes under visible light irradiation [94]. A hydrothermal/sonication route is adopted for synthesizing hexagonal WO_3 nanocrystals with various morphologies and the enhanced activities towards photo electrocatalytic HER by Mohamed et al. [95]. Adopting different synthesis parameters and precursors generated nano rod, nanosphere and nanotube morphology. Among which nanotube exhibited the highest efficacy of HER in the presence of light. The exposure of particular plane (411) and (112), oxygen vacancies and nanotube morphology obtained by the hydrothermal method plays a noteworthy role in the catalytic activity. This implies that the hydrothermal approach plays an important role in photocatalysis since it is less energy demanding; regulated, and convenient to use, with the ability to customize the shape and size in the 10–100 nm range.

3.1.3. Sol-Gel Synthesis

The sol-gel method is a popular procedure for fabricating materials such as thin films, inorganic nanoparticles, metal oxides, and other functional materials. Graham Thomas devised this process in 1864 for the manufacture of silica gels [96]. The field rapidly gained interest, with significant contributions from notable researchers.

A “sol” is a colloidal suspension of very minute solid particles (1–1000 nm) dispersed in an aqueous medium that are held together by short-range van der Waals forces. This process uses a sequence of chemical events to turn a sol into a gel-like network that includes both solid and liquid phases. This process is broadly categorized into two types: aqueous and non-aqueous. The sol-gel method is highly valued for its ability to create materials with large surface areas and stable surfaces. These characteristics are essential because the physical and chemical properties of the synthesized materials are considerably influenced by the experimental conditions that are employed during the process. The sol-gel synthesis generally includes the following sequential steps [97,98].

Hydrolysis and Polycondensation: Precursors such as metal alkoxides undergo hydrolysis in water or alcohol, followed by condensation reactions where water or alcohol is eliminated, forming metal oxide linkages. These reactions lead to the growth of polymeric networks and colloidal particles in the liquid state.

Gelation: As condensation progresses, the solution’s viscosity increases, and there is the generation of a porous gel structure in the liquid phase.

Aging: During this phase, polycondensation continues, along with localized precipitation within the gel network. This procedure decreases porosity and augments the thickness of the layer that separates colloidal particles.

Drying: This critical step involves removing water and organic components from the gel to form a solid material. Structural dispersion is minimized by different drying methods like supercritical, thermal and freeze drying.

The sol-gel process is particularly effective for synthesizing uniform, and homogeneous compositions [99–101]. This method’s capacity to generate mixed matrices is a significant advantage by carefully combining multiple metal oxide precursors. The parameters in this process such as the precursor type and solution’s pH, have an important part in the size and cross-linking of the resulting colloidal particles. In their study, Nagarjuna et al. used the sol-gel method to make WO_3 for the first time. This opens the door to large-scale production of supported oxides. The authors investigated the chemical changes, calcination temperature, structural evolution, and surface characteristics of WO_3 powders produced using this method. The synthesized WO_3 materials were employed to assess the photoreduction of the model priority pollutant, Cr(VI), under visible light [102].

3.1.4. Solution Combustion Method

Solution combustion is a promising technology that requires self-sustaining exothermic reactions in an aqueous or sol-gel environment. A wide range of nanomaterials, oxides, alloys, sulphides as well as inorganic ceramics and

composites with tailored properties, can be synthesised with this method. These materials find applications across various fields, such as catalysis, photocatalysis, electrocatalysis, heavy metal removal, sensors, and electronics. The technique's remarkable versatility and efficiency have led to the development of numerous variants, facilitating significant improvements in the quality and functionality of the synthesized materials [103,104]. Researchers explored photocatalytic properties of nanoscale WO_3 is synthesized utilizing an ultra-rapid solution combustion process with various fuels [105]. The fuels are glycerine, urea, citric acid *etc.* This synthesis process produced nanoparticles of various shapes, such as rods, spheres, needles *etc.* depending upon the fuel and amount of fuel. The synthesized method exhibited a considerable rate of photocatalytic performance towards methylene blue degradation.

3.2. WO_3 Based Photocatalysts for HER

3.2.1. Bare WO_3

WO_3 is a highly versatile material with several advantages, including its low fabrication cost and abundant availability. Its ability to be fabricated as thin films or coatings makes it particularly appealing for photocatalytic HER. In its bulk monoclinic form, WO_3 possesses an indirect band gap of 2.62 eV, harnessing around 12% of the solar spectrum's energy. This property makes it ideal for applications, such as photoelectrochemical cells, CO_2 photoreduction, and photocatalytic pollutants degradation. Significant research has taken place throughout the last three decades that has been dedicated to nanoscale structural control of tungsten oxide to enhance its photocatalytic performance. The blue colour of substoichiometric tungsten oxides is caused by the existence of defect states below the CB minimum. The defect states enable lower-energy excitations to the conduction band, leading to significant light absorption in the near-infrared spectrum. This phenomenon is primarily attributed to the excitation of free electrons in the conduction band, which originate from oxygen vacancies [106]. Paik et al. synthesized sub-stoichiometric tungsten oxide nanowires, typically ranging from 50 to 250 nm in length and possessing a diameter of less than 5 nm, exhibiting a dark navy-blue colour due to oxygen deprivation, by a high-temperature nonaqueous colloidal technique [107]. The presence of oxygen vacancies in the as-synthesized WO_3 nanowires (NWs) causes wide absorption from visible to infrared wavelengths. WO_3 NWs have a higher optical band gap (2.69 eV) than stoichiometric bulk WO_3 (3.05 eV). Photocatalytic hydrogen synthesis by photo reforming involves distributing nano particles in water/alcohol combinations and exposing them to UV/vis light. 1 wt% Pt serves as a co-catalyst on the WO_X NWs to enhance the kinetics of H_2 molecule production and function as an electron collector. The catalyst under UV/vis light exhibited hydrogen evolution of 464 μmol h^{-1} g^{-1} while bulk powder only produced less than 20 μmol h^{-1} g^{-1}. Researchers also examined ethanol, methanol, and glycerol as sacrificial agents. Figure 5c shows that H_2 evolution happens at about comparable rates in the occurrence of methanol and ethanol, however it befalls at half the rate in the presence of glycerol. The diminished rate of H_2 production in the presence of glycerol can be attributed to the substantial size of this sacrificial reagent within the photo reforming reaction, as well as the existence of secondary hydroxyl groups in glycerol.

The concept of oxygen vacancies in WO_3 renders it a compelling candidate for water splitting, as proposed by Wang et al. [108]. A straightforward room-temperature solution processing method has been disclosed, which has the potential to alter the surface morphology and electrical structure of WO_3, enabling an extraordinary ability to promote photocatalytic HER without relying on a co-catalyst. Surface disordered layer was created using a disordering agent Li-ethylenediamine (Li-EDA). A moderate gap band state was established, resulting in a blue shift of both the CBM and the E_f in comparison to the bare WO_3 (Figure 5d). Li-EDA treated WO_3(LT-WO_3) with new band structures exhibited photocatalytic HER of about 94.2 μmol h^{-1} g^{-1} under natural light without the assistance of a co-catalyst and was stable for 25 h (Figure 5e).

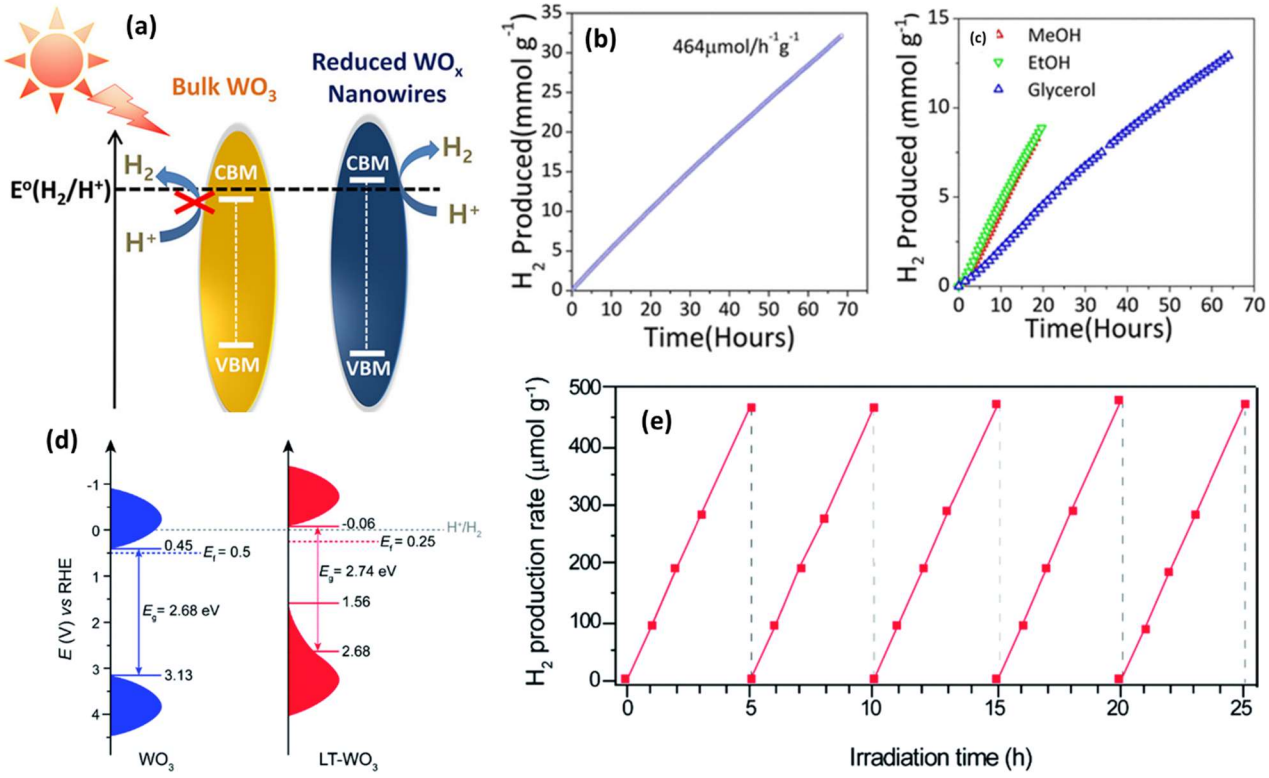

Figure 5. (**a**) Schematic representation of band shift from bulk to nano (**b**) Hydrogen production from 1 wt% Pt-loaded WO_x NWs under UV/vis light illumination in 1:1 vol. MeOH/H_2O mixture (**c**) Hydrogen evolution using a Pt/WO_x NW catalyst in sacrificial agents [107]. Copyright 2018. American Chemical Society. (**d**) Energy levels diagram of WO_3 and LT-WO_3 nanoplates (**e**) H_2 production rate from LT-WO_3 of 5 cycles in 25 h each [108]. Copyright 2019. Royal Society of Chemistry.

WO_3 presents limitations, such as rapid recombination of photogenerated charge carriers and a lower CB level that surpasses the reduction potential of O_2/O_2^-, leading to diminished O_2 molecule reduction during pollutant degradation via photocatalysis. This setback has prompted the search for acceptable methods to overcome these challenges, such as changing and regulating the structure of the semiconductor and lowering the band gap for improved photocatalysis via its production pathway and alternative improvement strategies. One such strategy was phase engineering that can actively tune the activity of photocatalysts by altering their band structure and active site configuration. Zhang et al. adjusted the precursor ratio for the synthesis of WO_3 by controlling phase changes [109]. Oxygen vacancies were persuaded in WO_3 at a relatively low temperature, resulting in the transition of crystal structure from monoclinic to orthorhombic or pseudo cubic phase. Orthorhombic and pseudo cubic WO_3 exhibited photocatalytic HER activities with 268 and 340 µmol g^{-1} h^{-1} H_2 generation rates respectively, while monoclinic didn't show any activity (Figure 6). Pseudo cubic WO_3 was stable for 24 h without any noticeable degradation in the catalytic activity. Reduced orthorhombic and pseudo cubic WO_3 emerged from vacancy generated WO_3 leading to WO_6 octahedra distortion. These alterations push the CBM over H_2 reduction potentials and enhancing the photocatalytic HER activity.

Another modification is substitutional doping of WO_3 with a suitable dopant material, which results in a favorable shift in band-edge location and narrowing of the band gap, hence boosting photocatalytic efficiency. Metal doping has been one of the prime strategies to overcome the demerits of WO_3 as a photocatalyst. Cu doped WO_3 was established to be an excellent photocatalysts for HER by Yin et al. [110]. The authors synthesized WO_3@Cu core-shell nanoparticles via sol–gel method. Copper served as an electron donor, increasing electron transfer efficiency and separating photogenerated electron-hole pairs, resulting in an H_2 generation rate of 37.78 µmol h^{-1} g^{-1} in visible light illumination.

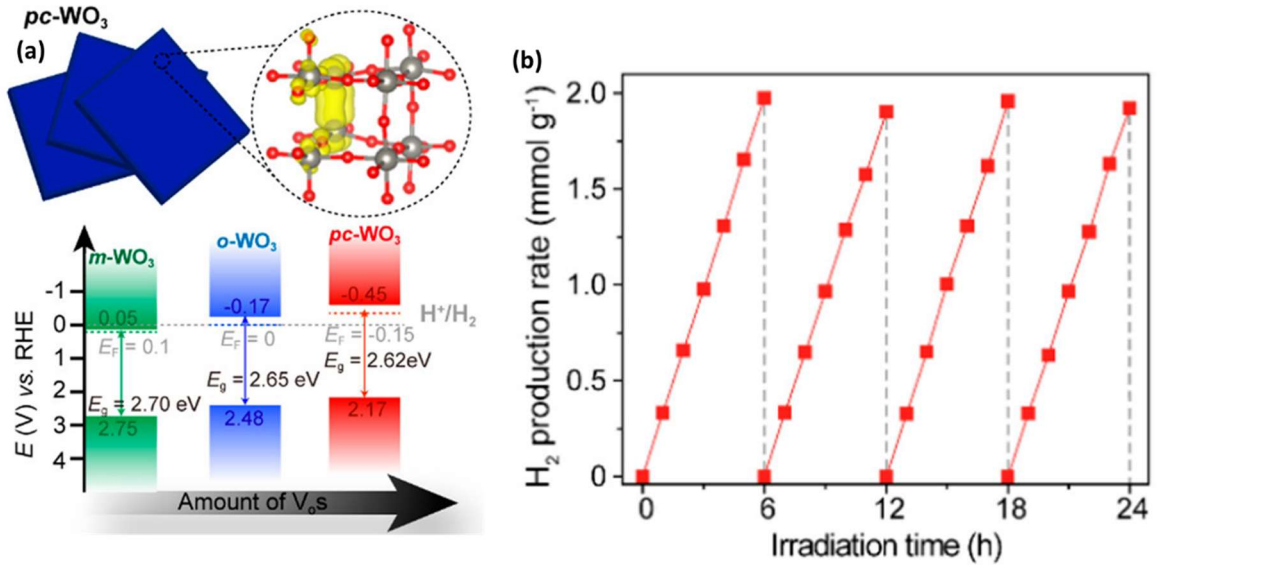

Figure 6. (**a**) Pseudo cubic WO_3 and band diagram of WO_3 of monoclinic, orthorhombic and pseudo cubic (**b**) HER activity of pseudo cubic-WO_{3-x} for 24 h reaction in four cycles. [109]. Copyright 2019. American Chemical Society.

3.2.2. Composites of WO_3

With Metal Oxides and Metal Sulphides

The extensive band gap, coupled with the unfavourable positioning of the band edges in WO_3, constrains the absorption of incident light and diminishes its efficacy in H_2 production. The VB edge of WO_3 is positive but CB edge is not negatively positioned compared to the redox potential of H_2 generation. This reduces the capability of H_2 production in the presence of light. In this scenario, the main method to overcome this is structural modification.

The key modification in forming heterojunction was with the most prominent and established photocatalyst TiO_2. This combination is perfect because it has a smaller bandgap than TiO_2 and a more positive conduction band edge. So, it can act as an electron trap, making charge separation work better and slowing the recombination of photogenerated carriers. One such combination was done by Camacho et al., where the researchers adopted sol-gel method to produce WO_3 in different molar ratios with TiO_2 nanoparticles. Further Pd metal was included in the TiO_2/WO_3 system [111]. Pd acted as an electron trapper promoting the photocatalytic activity. The motive of this study was the formation of TiO_2/WO_3 and the combination of Pd to enhance the light absorption to the visible region. It was observed that 0.001 wt% Pd TiO_2/WO_3 exhibited significant hydrogen generation of 7.7% quantum yield in water-methanol mixture. Another method adopted was composite formation of morphologically modified WO_3 with TiO_2. Quantum dots of WO_3 on TiO_2 were made using solvothermal and hydrogen-reduction techniques. These caused oxygen vacancy flaws to form in WO_3 [112]. These flaws kept TiO_2 and WO_{3-x}'s strong reductive and oxidative abilities while changing the charge-transfer route from type II heterojunction to Z-scheme. (Figure 7a,b). This enhanced the photocatalytic HER activity with the rate of 17.7 mmol h^{-1} g^{-1}.

To enhance photocatalytic activity, researchers have successfully produced a nanocomposite of TiO_2 core/TiO_2-WO_3 with core shell structure using acid precipitation preceded by thermal breakdown. TiO_2-WO_3 weight ratio was optimized to enable effective absorption of visible light. The hydrophilic nature of the composite enhanced water-splitting application. The coupled heterojunction in the shell structure facilitated the separation of charge carriers through the interaction of the Fermi levels of the shell components. With diethylamine hydrochloride, this procedure allowed electrons to migrate to the surface of the catalyst to generate 19.8 mL of hydrogen in one hour. The same group explored a multi-component n-n heterojunction consisting of WO_3, TiO_2, and Fe_2O_3 [113]. This approach leverages the synergistic interactions across the heterojunctions, significantly boosting photocatalytic performance. WO_3 nanoparticles particularly help to boost visible light absorption, hence increasing the activity. The aforementioned group of researchers integrated semiconductors to create n-n heterojunctions between Fe_2O_3 and TiO_2 on one side, whereas TiO_2 and WO_3 on the other side, resulting in n-n heterojunctions. The tri-component photocatalytic system with WO_3 nanoparticles at Fe_2O_3 and TiO_2 interfaces suppressed electron-hole recombination quite well (Figure 7c). WO_3 nanoparticles on Fe_2O_3 and TiO_2 surfaces adjusted the visible light band gap to 2.10 eV with hydrogen generation of 10.2 mL/h. CdO also has been considered to have incredible effect on WO_3 by altering its band gap. The presence of CdO makes the WO_3 more effective by promoting the charge separation and dropping the over potential of hydrogen

evolution. The presence of CdO tuned the crystallite size of WO_3 producing excellent photocatalytic hydrogen production [114].

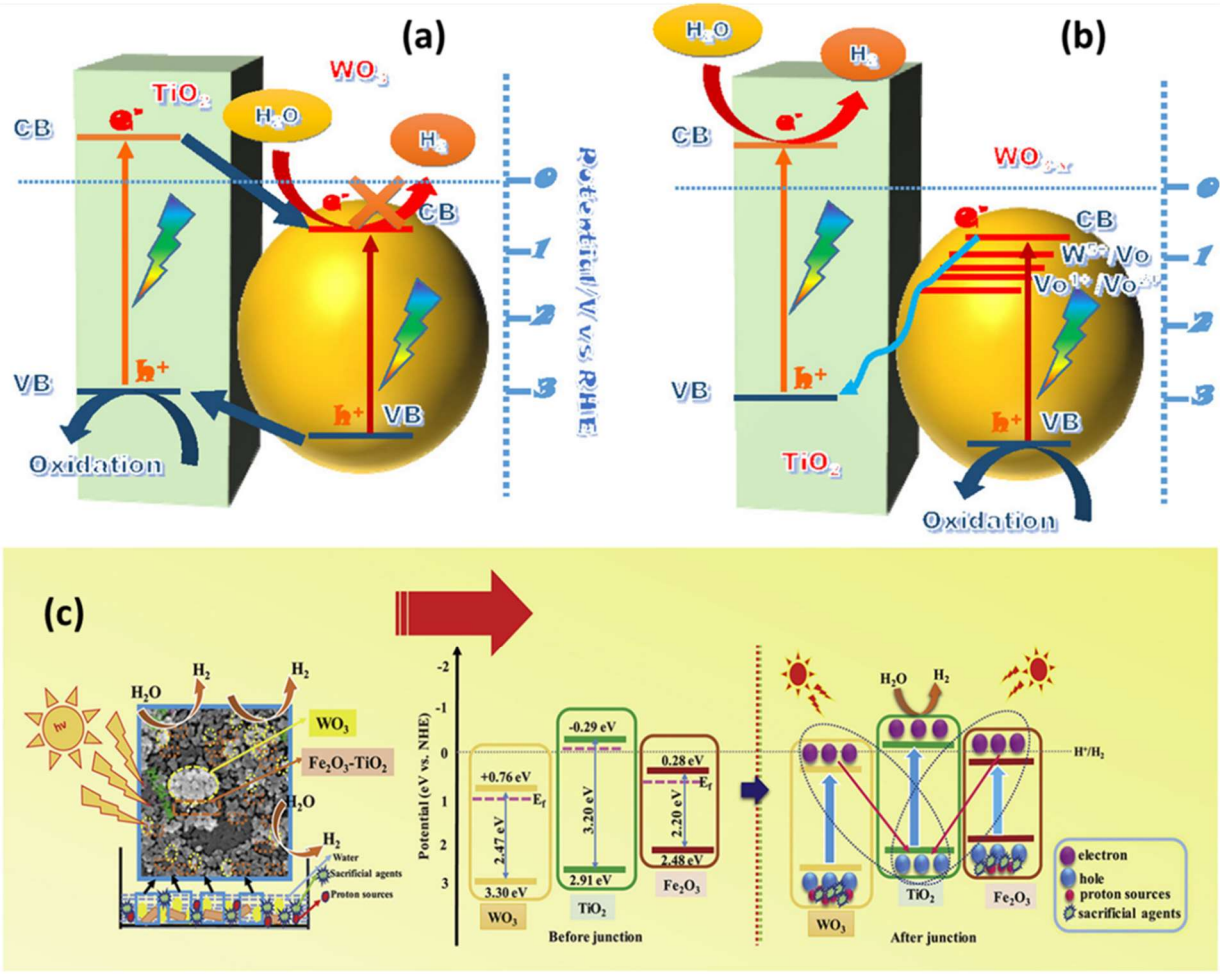

Figure 7. Z-scheme structure of (**a**) WO_3/TiO_2 and (**b**) WO_{3-x}/TiO_2 [112] Copyright 2017. Elsevier and (**c**) Scheme showing plausible mechanism describing the separation of charge carriers in the $WO_3/TiO_2/Fe_2O_3$ nano photocatalyst [113]. Copyright 2020, Elsevier.

Metal sulphides have also been explored for enhancing photocatalytic HER properties of WO_3. Some of the most prominent metal sulphides used along with WO_3 are CdS, Ag_2S, SnS_2, $ZnIn_2S_4$. A group of researchers explored the combination of WO_3 and CdS to achieve Z-scheme mechanism for photocatalytic HER under visible light irradiation [115]. The group used lactic acid as an electron donor. This combination enhanced the overall photocatalytic activity 5 times higher than CdS with the HER rate of 369 μmol h^{-1} g^{-1} with 20 wt% of CdS to WO_3. The presence of CdS with WO_3 results in the transfer of electrons from CdS to WO_3. Then, the interface band bending is moulded which results in potential barrier. On exposure of catalyst to light, electrons from CB of CdS cross the potential barrier can travel to WO_3. The photogenerated electrons in WO_3 combine with CdS holes. This makes it much less likely that photogenerated charge recycling will happen. More photogenerated electrons in CdS are available to reduce H^+ to H_2, which makes the photocatalytic H_2 evolution activity very strong. The same combination of composite was modified by another group in 2019 incorporating oxygen vacancies along with MoS_2 as cocatalyst for photocatalytic HER. The group tuned the concentration of WO_3 and cocatalyst MoS_2 along with synthesis time for high efficacy creating oxygen vacancy [116]. The existence of vacancies significantly enhanced light-capture capacity and promoted the transit of electrons and holes. H_2 generation was 2852.5 μmol g^{-1} h^{-1} for vacancy enriched CdS/WO_3 which was way better than bare CdS/WO_3 as mentioned in previous work. CdS-DETA has been synthesised by intercalating DETA organic molecules with CdS and incorporated to WO_3 as a direct Z scheme composite by solvothermal method. This improved the active sites and surface area for the favourable nanojunction structure, resulting in H_2 generation of 15,522 μmol/g h. Better H_2 evolution by photocatalysis is caused by the direct Z-scheme and the effective separation of electrons and holes. Separating electrons and holes in Z-scheme heterojunction composites stops holes from building up in the valence band of CdS due to WO_3. This stops CdS from corroding in sunlight and boosts photocatalytic activity [117].

With Metal Free Carbon Materials

Carbon materials' physio-chemical, electrical, and optical characteristics have been shown to vary depending on their many allotropic forms [17,118]. g-C_3N_4, an inorganic polymer has attained the greatest attention towards photocatalytic activity in the recent times. When g-C_3N_4 is combined with WO_3, a nanocomposite following Z scheme was made that works well as a photocatalyst when visible light hits it [119]. The great efficiency of WO_3/g-C_3N_4 composites in photocatalytic processes for hydrogen generation has attracted a lot of interest. A lot of work has been conducted on composites of WO_3/g-C_3N_4 with varied loading concentrations of WO_3, which include 2D g-C_3N_4/WO_3 composites, composites of both 2D g-C_3N_4 and 2D WO_3 *etc.* One such work was pyrolysis method for the synthesis of WO_3/g-C_3N_4 composites by varying WO_3 contents [120]. As WO_3 content was enhanced, the photocatalytic activity also increased 15 times than the pristine g-C_3N_4 with a rate of 400 μmol h^{-1} $g^{-1}c_{at}$ (Figure 8b). Optimising WO_3 to g-C_3N_4 and decreasing photogenerated charge carrier recombination led to the Z scheme and increased hydrogen generation. Morphologically modified g-C_3N_4/WO_3-carbon microsphere also has prominent impact on photocatalytic HER. Because g-C_3N_4/WO_3 and carbon microspheres work together so well, the g-C_3N_4/WO_3-carbon microsphere showed great hydrogen generation photocatalytic activity [121]. On the g-C_3N_4/WO_3-carbon microsphere hybrid photocatalyst, the g-C_3N_4 and WO_3 parts formed a Z-scheme heterojunction. This set-up shows that g-C_3N_4 and WO_3 can both make electrons and holes in the CB and VB, which results in a hydrogen generation rate of 1636.0 μmol h^{-1} g^{-1}. Carbon microspheres also work as charge transfer tunnels, speeding up the movement of photogenerated electrons and making it harder for photogenerated electron-hole pairs to combine again. The addition of NiS represented an alternative approach to improving the photocatalytic hydrogen evolution reaction performance of g-C_3N_4/WO_3. [122]. The growth of NiS-WO_3 in g-C_3N_4 changes its electronic structure and how its carriers behave. This NiS-assisted WO_3/g-C_3N_4 heterojunction system introduces additional active sites, enhancing the formation of heterojunctions and significantly improving charge separation and transfer efficiency enhancing the hydrogen production rate up to 2929.1 μmol/g h. The two main characteristics for this enhanced hydrogen production are that WO_3/g-C_3N_4 heterojunction suppressed the recombination rate and NiS provided more active sites as well as improved the electron mobility.

In 2018, a different group successfully made a heterojunction of WO_3/g-C_3N_4 as a 2D photocatalyst. The heterojunction has WO_3 nanoparticles that are 5 to 80 nm in size evenly placed on 2D g-C_3N_4 nanosheets using a hydrothermal method [123]. The composite demonstrated superior H_2 efficacy compared to pure g-C_3N_4 and WO_3, achieving an H_2 generation rate of 1853 μmol h^{-1} g^{-1} with Pt as a co-catalyst. Because of the creation of 2D nano-architectures and the way that WO_3 and g-C_3N_4 work together, the 2D WO_3/g-C_3N_4 photocatalyst is better at making H_2. This is because there are more active sites on the photocatalyst surface. By making the Z-scheme, it was also possible to limit the mixing of photoexcited electrons and holes while increasing the range of visible light that could be absorbed.

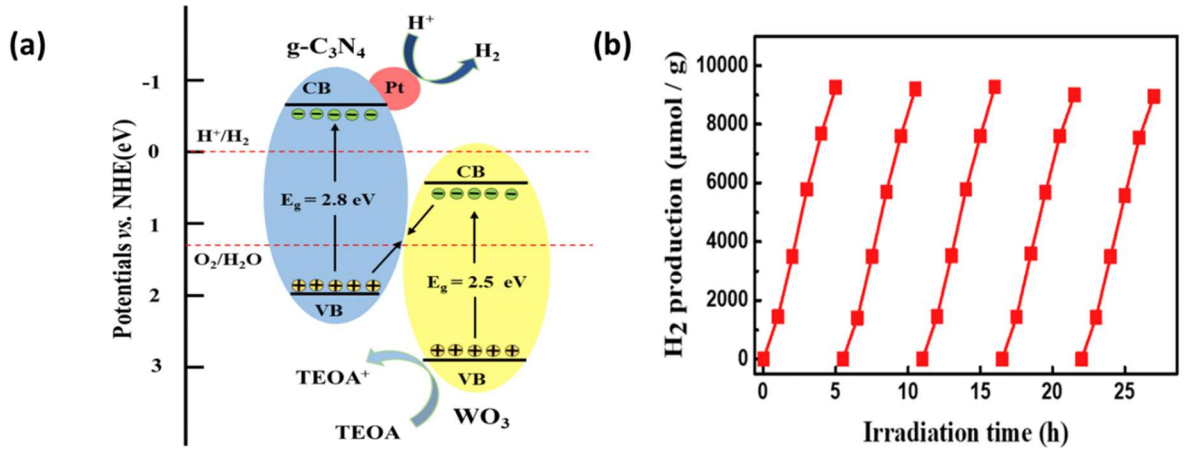

Figure 8. (**a**) Schematic diagram showing Z-scheme photocatalytic H_2-evolution mechanism for the WO_3/g-C_3N_4 composite (**b**) Cycle study for photocatalytic HER [123]. Copyright 2018, Elsevier.

Fu et al. designed a photocatalyst of WO_3 and g-C_3N_4 in 2D level [124]. The authors made a step-like heterojunction photocatalyst out of 2D/2D WO_3 and g-C_3N_4 by letting the WO_3 and g-C_3N_4 nanosheets stick together on their own. The obtained 2D/2D WO_3/g-C_3N_4 photocatalysts with Pt as the cocatalyst exhibited better H_2-production activity with the rate of 982 μmol h^{-1} g^{-1} than g-C_3N_4 and WO_3. The researchers clarified the mechanism by which, following intimate contact between g-C_3N_4 and WO_3, electrons from g-C_3N_4 were transferred to WO_3 across their interface until equilibrium of their Fermi levels was attained, leading to a positive charge on g-C_3N_4. Concurrently, WO_3 attains a

negative charge at the interface. Band edge of g-C_3N_4 has an upward curvature due to electron depletion, while WO_3 has a downward curvature. Light stimulated WO_3 and g-C_3N_4 electrons from VB to CB. The internal electric field, band edge bending, and coulombic interactions favor the recombination of some electrons (from WO_3's CB) with holes (from g-C_3N_4 VB) and inhibit others. The heterojunction mechanism using the S scheme removed less efficient electrons from WO_3's conduction band and holes from g-C_3N_4's valence band. The enhanced charge carrier transfer method significantly increased the redox capacity of the 2D/2D WO_3/g-C_3N_4 composite heterojunction, establishing it as an effective catalyst for hydrogen generation (Figure 9).

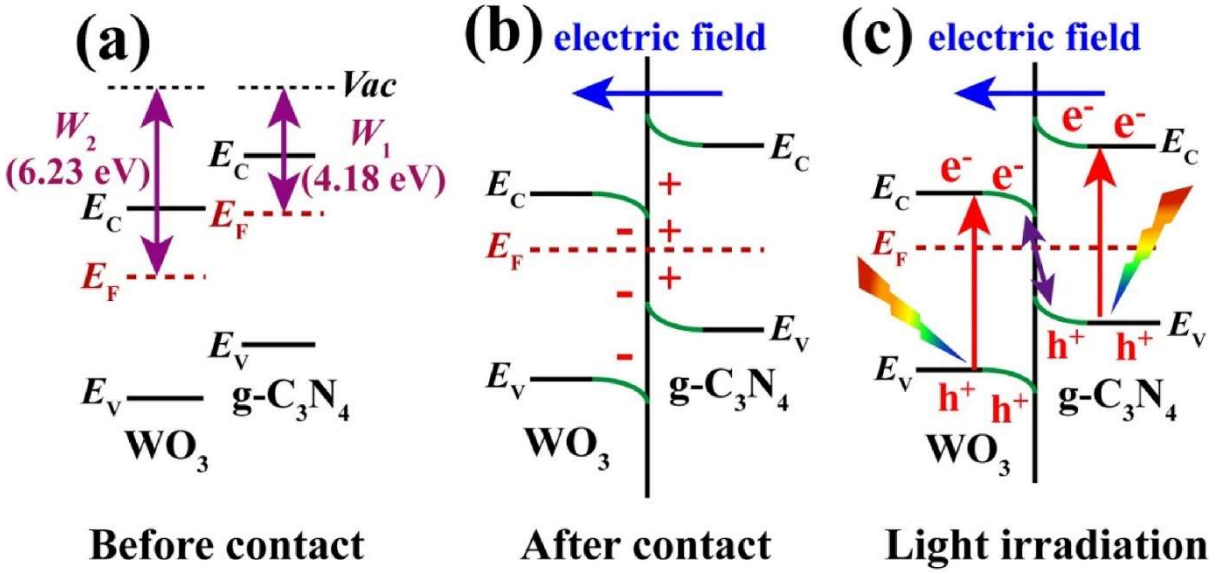

Figure 9. (**a**) g-C_3N_4 and WO_3 work function before contact. (**b**) Band edge bending and internal electric field at the interface of WO_3/g-C_3N_4 after contact. (**c**) The S-scheme charge transfer mechanism [124]. Copyright 2019, Elsevier.

Graphene is a candid 2D photocatalysts with high chemical stability and large surface-area. The 2D structure and exceptional physical-chemical properties, make it a profound candidate in photocatalytic applications. Integrating WO_3 with graphene to form multicomponent heterojunctions can lead to the development of effective photocatalysts. This combination facilitates efficient charge separation and minimizes the rate of photo-induced charge recombination, attributed to graphene's high specific surface area, rapid electron mobility, and excellent optical transparency. Tahir et al. successfully incorporated graphene into WO_3 through hydrothermal treatment, resulting in a composite with exceptional photocatalytic activity for H_2 generation [125]. 7% graphene significantly reduced recombination of electron-hole and enhanced reduction reactions, achieving a hydrogen evolution rate of 288 μmol h^{-1} g^{-1}. The better photocatalytic performance is due to the mutual interactions between graphene and WO_3. These interactions include WO_3 absorbing more visible light, having a larger surface area, and effectively separating charges.

Another group incorporated graphene nanoplates into TiO_2/WO_3 nanocomposite and investigated its photocatalytic properties towards H_2 generation [126]. The incorporation of graphene enhanced the transport and lifetime of photo-generated excitons, explicitly showing H_2 generation of 15 μmol/g_{cat} with 15 mol% of WO_3. This enhanced H_2 generation was anticipated because of the formation of type II heterojunction as shown in Figure 10. For type-II heterojunctions, the VB of WO_3 was less than that of TiO_2 where photogenerated holes in the VB of WO_3 can migrate to VB of TiO_2. Conversely, when CB of TiO_2 exceeds that of WO_3, electrons in the TiO_2 CB transfer to the WO_3 CB, leading to a spatial separation of electrons and holes. This may lead to a reduction in charge carrier recombination and an increase in charge carrier lifespan. A comprehensive list of composites of WO_3 along with their performances is provided in Table 1.

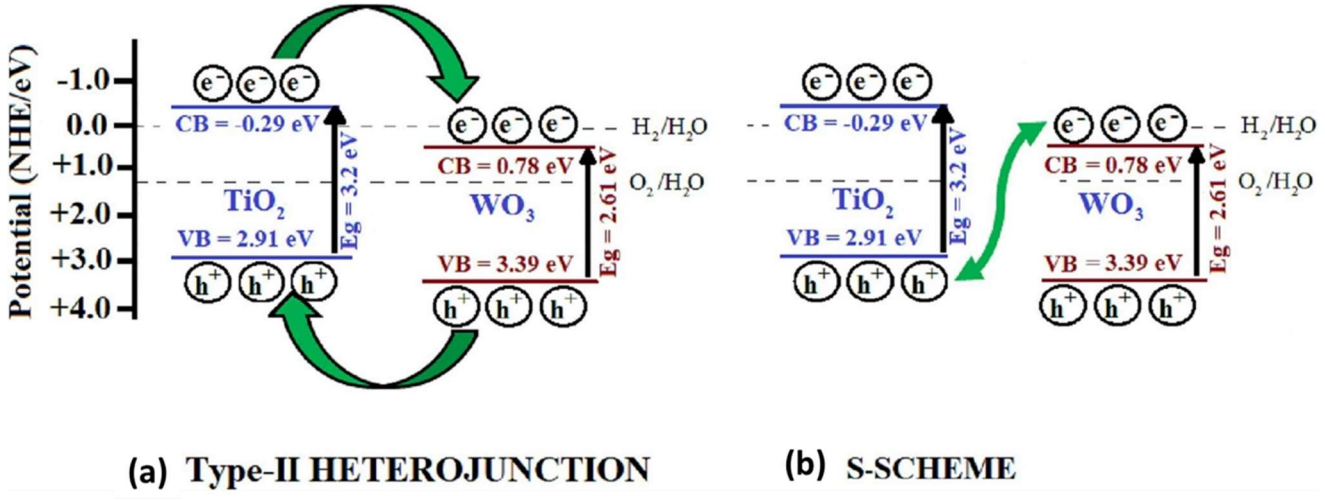

Figure 10. (**a**) Type–II heterojunction (**b**) S–scheme of TiO_2/WO_3 in UV light irradiation [126]. Copyright 2023, Elsevier.

Table 1. List of WO_3 and its composites along with their photocatalytic HER performances.

Sl No.	Photocatalysts	Light Source	Solvent	H_2 Rate (μmol h^{-1} g^{-1})	Ref.
1	WO_x NWs	150 W Hg-Xenon lamp	MeOH/H_2O (1:1)	464	[107]
2	LT-WO_3	150 W Xenon lamp	Na_2S/Na_2SO_3	94.2	[108]
3	WO_{3-x}	150 W Xenon lamp	Na_2S/Na_2SO_3	340	[109]
4	$WO_3/TiO_2/Fe_2O_3$	Solar Light	H_2O	10.2 mL/h	[113]
5	WO_3@Cu	400 W Hg lamp	MeOH/H_2O	37.78	[110]
6	Pd/TiO_2-WO_3	Solar simulator	MeOH/H_2O	5.3×10^{-5} mol/min g_{Cat}	[111]
7	WO_{3-x}QDs/TiO_2	Xenon lamp	methanol/H_2O	17.7 mmol h^{-1} g^{-1}	[112]
8	Pd/WT	UVP mercury lamp	90:10 H_2O/methanol	5427.0	[127]
9	$ZnIn_2S_4/WO_3$	Xenon lamp—300 W	10% methanol/H_2O	300	[128]
10	CuCl/WO_3	Xenon lamp—300 W	10% methanol/H_2O	15.8 μmol h^{-1}	[129]
11	TiO_2|Ti|WO_3	Xenon lamp—300 W	MeOH/H_2O	473.2 μmol	[130]
12	5 wt% $WO_3/ZnIn_2S_4$	Xenon lamp—300 W	Na_2S + Na_2SO_3	1945.8	[131]
13	2 mol% Ag/WO_3	Xenon arc lamp	H_2O	3	[132]
14	WO_3@MoS_2/CdS	Xenon lamp—300 W	10 vol.% of lactic acid	8.2	[133]
15	CuO-WO_3-CdS	300 W Xenon lamp	MB aqueous solution	178 μmol/g	[134]
16	WO_3-$Cd_{0.5}Zn_{0.5}S$	300 W Xenon lamp	Na_2S + Na_2SO_3	42.26 mmol h^{-1} g^{-1}	[135]
17	CN/HWO-Pt	300 W Xenon lamp	10 vol% TEOA/H_2O	862 μmol h^{-1}	[136]
18	p-gC_3N_4/WO_3 NTs	300 W Xenon lamp	Na_2S + Na_2SO_3	547	[137]
19	3% g-C_3N_4/WO_3	Visible light	H_2O	1425	[138]
20	7% graphene/WO_3	Metal-halide lamp	Na_2S + Na_2SO_3	288	[125]
21	WO_3@COF/rGO	300 W Xenon lamp	H_2O	26.7	[139]
22	$WO_3(H_2O)_{0.333}$/CdSe-DETA	300 W Xenon lamp	$Na_2S{\cdot}9H_2O$ + Na_2SO_3	2.4	[140]
23	WO_3-G	500 W Xe	10 vol% TEOA/H2O	400	[141]
24	WO_3/Ni–$ZnIn_2S_4$	Xe light source	Na_2S + Na_2SO_3	9.29 mmol h^{-1} g^{-1}	[142]
25	g-CN/WO_3/biochar/Cu^{2+}-Carbon	150 W Xe lamp	20 mL TEOA/H_2O	1900	[143]
26	g-C_3N_4/WO_3	350 W Xe lamp	H_2O	482 μmol h^{-1}	[144]

4. Conclusions and Future Perspective

In recent years, extensive studies were conducted on WO_3 and its composites for photocatalytic water splitting with respect to UV and visible light. The properties of WO_3 which include band gap, broad adsorption range, cost-effective preparation and stability in all harsh conditions, low cost and non-toxicity, make it a suitable candidate for photocatalytic water splitting. WO_3-based systems are better at photocatalysis because they can separate and transfer charges more efficiently. They also have a lot of surface area, which means they have lots of places for reactions to happen and help photogenerated charges move and separate quickly. The crucial factors governing the photocatalytic water splitting and H_2 generation are minimizing the recombination process and improving the number of active sites. Therefore, in this article, firstly in the introductory section, we have explicitly discussed the criteria and minutes of photocatalytic HER. Along with that, we tried to emphasize the assessment and various parameters that play a crucial role in photocatalytic H_2 generation.

We provided a detailed discussion on the properties of WO_3 and its various phases. The right way to make WO_3 and its strategies to boost visible light were found to be beneficial in helping to improve the separation and transfer of photogenerated charges, hence strengthening photocatalytic performance. Hence, we highlighted the impact of different synthesis methods, including sol-gel, solution combustion, and co-precipitation on its photocatalytic activity. Among these, the hydrothermal method is widely adopted, as it consistently produces photocatalysts with superior photocatalytic performance.

Finally, this review is dedicated to WO_3 and its composites with metals, metal oxides, and non-metals for photocatalytic HER. It explores the application of emerging S-scheme-based heterojunctions, efficient charge separation, and strong redox capabilities in various WO_3 composites. Although noteworthy and encouraging outcomes have been attained, additional meticulous refinement of the characteristics and structure of WO_3-based photocatalysts is essential to facilitate their practical deployment in real-world contexts. Despite these significant accomplishments, challenges still persist in this area. We propose several perspectives to advance the development of WO_3 as a photocatalyst for HER.

- In order to acquire a grasp of the mechanics of the reaction and optimisation of the reaction conditions for photocatalytic HER by WO_3, the fundamental aspects and kinetics should be revealed via theoretical studies.
- The improvement of enhancement levels and solar H_2 generation efficiency remains crucial for commercialization. This requires minimizing the recombination of photogenerated electron-hole pairs, extending their lifetime, and enhancing the adsorption of reactants.
- For effective water splitting involving WO_3 and its composites, along with optimized reactor and reaction conditions—such as temperature, sacrificial reagents, photocatalyst dosage, and light source—should be developed and made readily available for large-scale applications.

5. Dedication

This paper is devoted to the memory of Professor David F. Ollis, who left us on 6 October 2023. Professor Ollis, who was internationally known to everyone in our fields of science and engineering, was a leader in numerous areas of chemical engineering and technology as he performed breakthrough research and pioneered many new approaches that shaped the way we practice engineering. His research contributions were characterized by thoroughness and great breadth. Professor Ollis played a pivotal role in introducing biochemical engineering to numerous chemical engineering departments across the United States and around the world. Beyond his research, he was an extraordinary and devoted educator who deeply cared about his students and their learning. Professor David F. Ollis was a good friend and mentor of mine (P.G. Smirniotis), and he will be missed very much, but his work will stay with us forever.

Acknowledgments

The authors acknowledge University of Cincinnati for providing research infrastructure.

Author Contributions

P.C.M.: Original draft, Writing—review and editing. B.M.—Review and editing. P.G.S.: Supervision, review and editing.

Ethics Statement

Not applicable.

Informed Consent Statement

Not applicable.

Data Availability Statement

The data used in the review can be accessed through the cited publication within the manuscript.

Funding

This research received no external funding.

Declaration of Competing Interest

The authors declare that they have no known competing financial interests or personal relationships that could have appeared to influence the work reported in this paper.

References

1. Peter SC. Reduction of CO_2 to Chemicals and Fuels: A Solution to Global Warming and Energy Crisis. *ACS Energy Lett.* **2018**, *3*, 1557–1561.
2. Peters GP, Aamaas B, Lund MT, Solli C, Fuglestvedt JS. Alternative "Global Warming" Metrics in Life Cycle Assessment: A Case Study with Existing Transportation Data. *Environ. Sci. Technol.* **2011**, *45*, 8633–8641.
3. Christoforidis KC, Fornasiero P. Photocatalytic Hydrogen Production: A Rift into the Future Energy Supply. *ChemCatChem* **2017**, *9*, 1523–1544.
4. Nguyen TP, Tuan Nguyen DM, Tran DL, Le HK, Vo D-VN, Lam SS, et al. MXenes: Applications in Electrocatalytic, Photocatalytic Hydrogen Evolution Reaction and CO_2 Reduction. *Mol. Catal.* **2020**, *486*, 110850.
5. Sha MA, Mohanan G, Elias L, Bhagya TC, Shibli SMA. Boosting Charge Separation of CeO_2–MnO_2 Nanoflake with Heterojunctions for Enhanced Photocatalytic Hydrogen Generation. *Mater. Chem. Phys.* **2023**, *294*, 127019.
6. Meenu PC, Sha MA, Pavithran R, Dilimon VS, Shibli SMA. Stacked Nano Rods of Cobalt and Nickel Based Metal Organic Frame Work of 2–Amino Benzene Dicarboxylic Acid for Photocatalytic Hydrogen Generation. *Int. J. Hydrogen Energy* **2020**, *45*, 24582–24594.
7. Rahman MZ, Kibria MG, Mullins CB. Metal-Free Photocatalysts for Hydrogen Evolution. *Chem. Soc. Rev.* **2020**, *49*, 1887–1931.
8. Chu X, Sathish CI, Yang J-H, Guan X, Zhang X, Qiao L, et al. Strategies for Improving the Photocatalytic Hydrogen Evolution Reaction of Carbon Nitride-Based Catalysts. *Small* **2023**, *19*, 2302875.
9. Krishnan AA, Kumar A, Nair RB, Sivaraj R, Lamiya A, Jishnu PK, et al. Multifunctional Na-Enriched Ni–Fe/Ni–P Plates for Highly Efficient Photo- and Electrocatalytic Water Splitting Reactions. *New J. Chem.* **2022**, *46*, 22256–22267.
10. Fujishim AA, Honda K. Electrochemical Photolysis of Water at a Semiconductor Electrode. *Nature* **1972**, *238*, 37–38.
11. Abhishek B, Jayarama A, Rao AS, Nagarkar SS, Dutta A, Duttagupta SP, et al. Challenges in Photocatalytic Hydrogen Evolution: Importance of Photocatalysts and Photocatalytic Reactors. *Int. J. Hydrogen Energy* **2024**, *81*, 1442–1466.
12. Beil SB, Bonnet S, Casadevall C, Detz RJ, Eisenreich F, Glover SD, et al. Challenges and Future Perspectives in Photocatalysis: Conclusions from an Interdisciplinary Workshop. *JACS Au* **2024**, *4*, 2746–2766.
13. Mohd Zaki RSR, Jusoh R, Chanakaewsomboon I, Setiabudi HD. Recent Advances in Metal Oxide Photocatalysts for Photocatalytic Degradation of Organic Pollutants: A Review on Photocatalysts Modification Strategies. *Mater. Today Proc.* **2024**, *107*, 59–67.
14. Graciani J, Nambu A, Evans J, Rodriguez JA, Sanz JF. Au ↔ N Synergy and N-Doping of Metal Oxide-Based Photocatalysts. *J. Am. Chem. Soc.* **2008**, *130*, 12056–12063.
15. Babu P, Naik B. Cu–Ag Bimetal Alloy Decorated SiO_2@TiO_2 Hybrid Photocatalyst for Enhanced H2 Evolution and Phenol Oxidation under Visible Light. *Inorg. Chem.* **2020**, *59*, 10824–10834.
16. Xiao Q, Sarina S, Waclawik ER, Jia J, Chang J, Riches JD, et al. Alloying Gold with Copper Makes for a Highly Selective Visible-Light Photocatalyst for the Reduction of Nitroaromatics to Anilines. *ACS Catal.* **2016**, *6*, 1744–1753.
17. Rosso C, Filippini G, Criado A, Melchionna M, Fornasiero P, Prato M. Metal-Free Photocatalysis: Two-Dimensional Nanomaterial Connection toward Advanced Organic Synthesis. *ACS Nano* **2021**, *15*, 3621–3630.
18. Payra S, Roy S. From Trash to Treasure: Probing Cycloaddition and Photocatalytic Reduction of CO_2 over Cerium-Based Metal–Organic Frameworks. *J. Phys. Chem. C* **2021**, *125*, 8497–8507.
19. Kaushal N, Taha AA, Tyagi S, Smirniotis PG. NH_2-MIL-101(Fe)/N-CNDs as a Visible Light Photocatalyst for Degradation of Fluoroquinolone Antibiotics in Water. *Mater. Chem. Phys.* **2025**, *332*, 130198.
20. Schneider J, Matsuoka M, Takeuchi M, Zhang J, Horiuchi Y, Anpo M, et al. Understanding TiO_2 Photocatalysis: Mechanisms and Materials. *Chem. Rev.* **2014**, *114*, 9919–9986.
21. Vorontsov AV, Valdés H, Smirniotis PG, Paz Y. Recent Advancements in the Understanding of the Surface Chemistry in TiO_2 Photocatalysis. *Surfaces* **2020**, *3*, 72–92.
22. Zheng X, Kuang Q, Yan K, Qiu Y, Qiu J, Yang S. Mesoporous TiO_2 Single Crystals: Facile Shape-, Size-, and Phase-Controlled Growth and Efficient Photocatalytic Performance. *ACS Appl. Mater. Interfaces* **2013**, *5*, 11249–11257.
23. Li X, Zheng W, He G, Zhao R, Liu D. Morphology Control of TiO_2 Nanoparticle in Microemulsion and Its Photocatalytic Property. *ACS Sustain. Chem. Eng.* **2014**, *2*, 288–295.
24. Tang H, Chang S, Wu K, Tang G, Fu Y, Liu Q, et al. Band Gap and Morphology Engineering of TiO_2 by Silica and Fluorine Co-Doping for Efficient Ultraviolet and Visible Photocatalysis. *RSC Adv.* **2016**, *6*, 63117–63130.
25. Khlyustova A, Sirotkin N, Kusova T, Kraev A, Titov V, Agafonov A. Doped TiO_2: The Effect of Doping Elements on

Photocatalytic Activity. *Mater. Adv.* **2020**, *1*, 1193–1201.
26. Tu B, Hao J, Wang F, Li Y, Li J, Qiu J. Element Doping Adjusted the Built-in Electric Field at the TiO_2/CdS Interface to Enhance the Photocatalytic Reduction Activity of Cr(VI). *Chem. Eng. J.* **2023**, *456*, 141103.
27. Pugazhenthiran N, Murugesan S, Valdés H, Selvaraj M, Sathishkumar P, Smirniotis PG, et al. Photocatalytic Oxidation of Ceftiofur Sodium under UV–Visible Irradiation Using Plasmonic Porous Ag-TiO_2 Nanospheres. *J. Ind. Eng. Chem.* **2022**, *105*, 384–392.
28. Smirniotis PG, Boningari T, Damma D, Inturi SNR. Single-Step Rapid Aerosol Synthesis of N-Doped TiO_2 for Enhanced Visible Light Photocatalytic Activity. *Catal. Commun.* **2018**, *113*, 1–5.
29. Qi K, Imparato C, Almjasheva O, Khataee A, Zheng W. TiO_2-Based Photocatalysts from Type-II to S-Scheme Heterojunction and Their Applications. *J. Colloid Interface Sci.* **2024**, *675*, 150–191.
30. Wei L, Yu C, Zhang Q, Liu H, Wang Y. TiO_2-Based Heterojunction Photocatalysts for Photocatalytic Reduction of CO_2 into Solar Fuels. *J. Mater. Chem. A* **2018**, *6*, 22411–22436.
31. Prabhu A, Meenu PC, Roy S. Creation of a Facile Heterojunction in Co/ZnO–TiO_2 for the Photocatalytic Degradation of Alizarin S. *New J. Chem.* **2024**, *48*, 10552–10562.
32. Muhmood T, Ahmad I, Haider Z, Haider SK, Shahzadi N, Aftab A, et al. Graphene-like Graphitic Carbon Nitride (g-C_3N_4) as a Semiconductor Photocatalyst: Properties, Classification, and Defects Engineering Approaches. *Mater. Today Sustain.* **2024**, *25*, 100633.
33. Fu J, Yu J, Jiang C, Cheng B. G-C_3N_4-Based Heterostructured Photocatalysts. *Adv. Energy Mater.* **2018**, *8*, 1701503.
34. Fujiwara T, Sasahara A, Happo N, Kimura K, Hayashi K, Onishi H. Single-Crystal Model of Highly Efficient Water-Splitting Photocatalysts: A $KTaO_3$ Wafer Doped with Calcium Cations. *Chem. Mater.* **2020**, *32*, 1439–1447.
35. Sasahara A, Kimura K, Sudrajat H, Happo N, Hayashi K, Onishi H. $KTaO_3$ Wafers Doped with Sr or La Cations for Modeling Water-Splitting Photocatalysts: 3D Atom Imaging around Doping Cations. *J. Phys. Chem. C* **2022**, *126*, 19745–19755.
36. Polisetti S, Deshpande PA, Madras G. Photocatalytic Activity of Combustion Synthesized ZrO_2 and ZrO_2–TiO_2 Mixed Oxides. *Ind. Eng. Chem. Res.* **2011**, *50*, 12915–12924.
37. Wang J, Huang J, Meng J, Li Q, Yang J. Double-Hole Codoped Huge-Gap Semiconductor ZrO_2 for Visible-Light Photocatalysis. *Phys. Chem. Chem. Phys.* **2016**, *18*, 17517–17524.
38. Trang TNQ, Tran Van M, Phan TB, Thu VTH. Spatially Controlled Photogenerated Charge Carriers Induced by $SrTiO_3$-Architectured Heterojunction Nanocubes for a Photocatalytic Hydrogen Evolution Reaction. *ACS Appl. Energy Mater.* **2021**, *4*, 8910–8921.
39. Kuang Q, Yang S. Template Synthesis of Single-Crystal-Like Porous $SrTiO_3$ Nanocube Assemblies and Their Enhanced Photocatalytic Hydrogen Evolution. *ACS Appl. Mater. Interfaces* **2013**, *5*, 3683–3690.
40. Linsebigler AL, Lu G, Yates JTJ. Photocatalysis on TiO2 Surfaces: Principles, Mechanisms, and Selected Results. *Chem. Rev.* **1995**, *95*, 735–758.
41. Zhao Y, Li R, Mu L, Li C. Significance of Crystal Morphology Controlling in Semiconductor-Based Photocatalysis: A Case Study on $BiVO_4$ Photocatalyst. *Cryst. Growth Des.* **2017**, *17*, 2923–2928.
42. Dai D, Liang X, Zhang B, Wang Y, Wu Q, Bao X, et al. Strain Adjustment Realizes the Photocatalytic Overall Water Splitting on Tetragonal Zircon $BiVO_4$. *Adv. Sci.* **2022**, *9*, 2105299.
43. Vemuri RS, Engelhard MH, Ramana CV. Correlation between Surface Chemistry, Density, and Band Gap in Nanocrystalline WO_3 Thin Films. *ACS Appl. Mater. Interfaces* **2012**, *4*, 1371–1377.
44. Dutta V, Sharma S, Raizada P, Thakur VK, Khan AAP, Saini V, et al. An Overview on WO_3 Based Photocatalyst for Environmental Remediation. *J. Environ. Chem. Eng.* **2021**, *9*, 105018.
45. Subramanyam P, Meena B, Sinha GN, Deepa M, Subrahmanyam C. Decoration of Plasmonic Cu Nanoparticles on WO_3/Bi_2S_3 QDs Heterojunction for Enhanced Photoelectrochemical Water Splitting. *Int. J. Hydrogen Energy* **2020**, *45*, 7706–7715.
46. Yao Y, Sang D, Zou L, Wang Q, Liu C. A Review on the Properties and Applications of WO_3 Nanostructure-based Optical and Electronic Devices. *Nanomaterials* **2021**, *11,* 2136.
47. Coridan RH, Shaner M, Wiggenhorn C, Brunschwig BS, Lewis NS. Electrical and Photoelectrochemical Properties of WO_3/Si Tandem Photoelectrodes. *J. Phys. Chem. C* **2013**, *117*, 6949–6957.
48. Abe R, Takata T, Sugihara H, Domen K. Photocatalytic Overall Water Splitting under Visible Light by TaON and WO_3 with an IO_3^-/I^- Shuttle Redox Mediator. *Chem. Commun.* **2005**, *30,* 3829–3831.
49. Ismail AA, Bahnemann DW. Photochemical Splitting of Water for Hydrogen Production by Photocatalysis: A Review. *Sol. Energy Mater. Sol. Cells* **2014**, *128*, 85–101.
50. Xing J, Jiang HB, Chen JF, Li YH, Wu L, Yang S, et al. Active Sites on Hydrogen Evolution Photocatalyst. *J. Mater. Chem. A* **2013**, *1*, 15258–15264.
51. Hai X, Zhou W, Chang K, Pang H, Liu H, Shi L, et al. Engineering the Crystallinity of MoS_2 Monolayers for Highly Efficient Solar Hydrogen Production. *J. Mater. Chem. A* **2017**, *5*, 8591–8598.
52. Xu M, Jiang L, Wang J, Feng S, Tremblay P-L, Zhang T. Efficient Photocatalytic Hydrogen Evolution with High-Crystallinity and Noble Metal-Free Red Phosphorus-CdS Nanorods. *Int. J. Hydrogen Energy* **2020**, *45*, 17354–17366.

53. Li D, Song H, Meng X, Shen T, Sun J, Han W, et al. Effects of Particle Size on the Structure and Photocatalytic Performance by Alkali-Treated TiO_2. *Nanomaterials* **2020**, *10*, 546.
54. Li X, Yu J, Low J, Fang Y, Xiao J, Chen X. Engineering Heterogeneous Semiconductors for Solar Water Splitting. *J. Mater. Chem. A* **2015**, *3*, 2485–2534.
55. Zhang Y, Ma D, Li J, Zhi C, Zhang Y, Liang L, et al. Recent Research Advances of Metal Organic Frameworks (MOFs) Based Composites for Photocatalytic H_2 Evolution. *Coord. Chem. Rev.* **2024**, *517*, 215995.
56. Ng KH, Lai SY, Cheng CK, Cheng YW, Chong CC. Photocatalytic Water Splitting for Solving Energy Crisis: Myth, Fact or Busted? *Chem. Eng. J.* **2021**, *417*, 128847.
57. Mei B, Han K, Mul G. Driving Surface Redox Reactions in Heterogeneous Photocatalysis: The Active State of Illuminated Semiconductor-Supported Nanoparticles during Overall Water-Splitting. *ACS Catal.* **2018**, *8*, 9154–9164.
58. Wu S, Sun J, Li Q, Hood ZD, Yang S, Su T, et al. Effects of Surface Terminations of 2D Bi_2WO_6 on Photocatalytic Hydrogen Evolution from Water Splitting. *ACS Appl. Mater. Interfaces* **2020**, *12*, 20067–20074.
59. Ricka R, Přibyl M, Kočí K. Apparent Quantum Yield-Key Role of Spatial Distribution of Irradiation. *Appl. Catal. A Gen.* **2023**, *658*, 119166.
60. Sakata Y, Hayashi T, Yasunaga R, Yanaga N, Imamura H. Remarkably High Apparent Quantum Yield of the Overall Photocatalytic H_2O Splitting Achieved by Utilizing Zn Ion Added Ga_2O_3 Prepared Using Dilute $CaCl_2$ Solution. *Chem. Commun.* **2015**, *51*, 12935–12938.
61. Cargnello M, Gasparotto A, Gombac V, Montini T, Barreca D, Fornasiero P. Photocatalytic H_2 and Added-Value By-Products-The Role of Metal Oxide Systems in Their Synthesis from Oxygenates. *Eur. J. Inorg. Chem.* **2011**, *2011*, 4309–4323.
62. Serpone N. Relative Photonic Efficiencies and Quantum Yields in Heterogeneous Photocatalysis. *J. Photochem. Photobiol. A Chem.* **1997**, *104*, 1–12.
63. Zhang L, Mohamed HH, Dillert R, Bahnemann D. Kinetics and Mechanisms of Charge Transfer Processes in Photocatalytic Systems: A Review. *J. Photochem. Photobiol. C Photochem. Rev.* **2012**, *13*, 263–276.
64. Guayaquil-Sosa JF, Serrano-Rosales B, Valadés-Pelayo PJ, de Lasa H. Photocatalytic Hydrogen Production Using Mesoporous TiO_2 Doped with Pt. *Appl. Catal. B Environ.* **2017**, *211*, 337–348.
65. Soundarya TL, Harini R, Manjunath K, Nirmala B, Nagaraju G. Pt-Doped TiO_2 Nanotubes as Photocatalysts and Electrocatalysts for Enhanced Photocatalytic H_2 Generation, Electrochemical Sensing, and Supercapacitor Applications. *Int. J. Hydrogen Energy* **2023**, *48*, 31855–31874.
66. Khorashadizade E, Mohajernia S, Hejazi S, Mehdipour H, Naseri N, Moradlou O, et al. Intrinsically Ru-Doped Suboxide TiO_2 Nanotubes for Enhanced Photoelectrocatalytic H_2 Generation. *J. Phys. Chem. C* **2021**, *125*, 6116–6127.
67. Li J, Yi D, Zhan F, Zhou B, Gao D, Guo D, et al. Monolayered Ru_1/TiO_2 Nanosheet Enables Efficient Visible-Light-Driven Hydrogen Evolution. *Appl. Catal. B Environ.* **2020**, *271*, 118925.
68. Chen D, Gao H, Yao Y, Zhu L, Zhou X, Peng X, et al. Pd Loading, Mn+ (N=1, 2, 3) Metal Ions Doped TiO_2 Nanosheets for Enhanced Photocatalytic H2 Production and Reaction Mechanism. *Int. J. Hydrogen Energy* **2022**, *47*, 10250–10260.
69. Chen Y, Soler L, Armengol-Profitós M, Xie C, Crespo D, Llorca J. Enhanced Photoproduction of Hydrogen on Pd/TiO_2 Prepared by Mechanochemistry. *Appl. Catal. B Environ.* **2022**, *309*, 121275.
70. Wang P, Pan J, Yu Q, Wang P, Wang J, Song C, et al. The Enhanced Photocatalytic Hydrogen Production of the Non-Noble Metal Co-Catalyst Mo_2C/CdS Hollow Core-Shell Composite with $CdMoO_4$ Transition Layer. *Appl. Surf. Sci.* **2020**, *508*, 145203.
71. Ma B, Wang X, Lin K, Li J, Liu Y, Zhan H, et al. A Novel Ultraefficient Non-Noble Metal Composite Cocatalyst Mo_2N/Mo_2C/Graphene for Enhanced Photocatalytic H2 Evolution. *Int. J. Hydrogen Energy* **2017**, *42*, 18977–18984.
72. Ran J, Zhu B, Qiao SZ. Phosphorene Co-Catalyst Advancing Highly Efficient Visible-Light Photocatalytic Hydrogen Production. *Angew. Chemie Int. Ed.* **2017**, *56*, 10373–10377.
73. Rezaei M, Nezamzadeh-Ejhieh A, Massah AR. A Comprehensive Review on the Boosted Effects of Anion Vacancy in the Photocatalytic Solar Water Splitting: Focus on Sulfur Vacancy. *Energy Fuels* **2024**, *38*, 7637–7664.
74. Kumar A, Krishnan V. Vacancy Engineering in Semiconductor Photocatalysts: Implications in Hydrogen Evolution and Nitrogen Fixation Applications. *Adv. Funct. Mater.* **2021**, *31*, 2009807.
75. Yu K, Huang HB, Wang JT, Liu GF, Zhong Z, Li YF, et al. Engineering Cation Defect-Mediated Z-Scheme Photocatalysts for a Highly Efficient and Stable Photocatalytic Hydrogen Production. *J. Mater. Chem. A* **2021**, *9*, 7759–7766.
76. Karimi Estahbanati MR, Mahinpey N, Feilizadeh M, Attar F, Iliuta MC. Kinetic Study of the Effects of PH on the Photocatalytic Hydrogen Production from Alcohols. *Int. J. Hydrogen Energy* **2019**, *44*, 32030–32041.
77. Hameed A, Gondal MA, Yamani ZH, Yahya AH. Significance of PH Measurements in Photocatalytic Splitting of Water Using 355nm UV Laser. *J. Mol. Catal. A Chem.* **2005**, *227*, 241–246.
78. Huaxu L, Fuqiang W, Ziming C, Shengpeng H, Bing X, Xiangtao G, et al. Analyzing the Effects of Reaction Temperature on Photo-Thermo Chemical Synergetic Catalytic Water Splitting under Full-Spectrum Solar Irradiation: An Experimental and Thermodynamic Investigation. *Int. J. Hydrogen Energy* **2017**, *42*, 12133–12142.
79. Baniasadi E, Dincer I, Naterer GF. Measured Effects of Light Intensity and Catalyst Concentration on Photocatalytic Hydrogen

and Oxygen Production with Zinc Sulfide Suspensions. *Int. J. Hydrogen Energy* **2013**, *38*, 9158–9168.
80. Guzman F, Chuang SSC, Yang C. Role of Methanol Sacrificing Reagent in the Photocatalytic Evolution of Hydrogen. *Ind. Eng. Chem. Res.* **2013**, *52*, 61–65.
81. Kumaravel V, Imam MD, Badreldin A, Chava RK, Do JY, Kang M, et al. Photocatalytic Hydrogen Production: Role of Sacrificial Reagents on the Activity of Oxide, Carbon, and Sulfide Catalysts. *Catalysts*. **2019**, *3*, 276.
82. Bowker M, Morton C, Kennedy J, Bahruji H, Greves J, Jones W, et al. Hydrogen Production by Photoreforming of Biofuels Using Au, Pd and Au–Pd/TiO2 Photocatalysts. *J. Catal.* **2014**, *310*, 10–15.
83. Pelayo D, Pérez-Peña E, Rivero MJ, Ortiz I. Shedding Light on the Photocatalytic Hydrogen Generation from Seawater Using CdS. *Catal. Today* **2024**, *433*, 114672.
84. Samuel O, Othman MHD, Kamaludin R, Sinsamphanh O, Abdullah H, Puteh MH, et al. WO_3–Based Photocatalysts: A Review on Synthesis, Performance Enhancement and Photocatalytic Memory for Environmental Applications. *Ceram. Int.* **2022**, *48*, 5845–5875.
85. Wang Z, Einaga H. WO_3-Based Materials for Photocatalytic and Photoelectrocatalytic Selective Oxidation Reactions. *ChemCatChem* **2023**, *15*, e202300723.
86. Chatten R, Chadwick AV, Rougier A, Lindan PJD. The Oxygen Vacancy in Crystal Phases of WO_3. *J. Phys. Chem. B* **2005**, *109*, 3146–3156.
87. Pihosh Y, Turkevych I, Mawatari K, Uemura J, Kazoe Y, Kosar S, et al. Photocatalytic Generation of Hydrogen by Core-Shell WO_3/$BiVO_4$ Nanorods with Ultimate Water Splitting Efficiency. *Sci. Rep.* **2015**, *5*, 11141.
88. Stankic S, Suman S, Haque F, Vidic J. Pure and Multi Metal Oxide Nanoparticles: Synthesis, Antibacterial and Cytotoxic Properties. *J. Nanobiotechnology* **2016**, *14*, 73.
89. Thilagavathi T, Venugopal D, Marnadu R, Chandrasekaran J, Thangaraju D, Palanivel B, et al. WO_3/$CoWO_4$ Nanocomposite Synthesis Using a Facile Co-Precipitation Method for Enhanced Photocatalytic Applications. *J. Phys. Chem. Solids* **2021**, *154*, 110066.
90. Banić ND, Abramović BF, Krstić JB, Šojić Merkulov DV, Finčur NL, Mitrić MN. Novel WO_3/Fe_3O_4 Magnetic Photocatalysts: Preparation, Characterization and Thiacloprid Photodegradation. *J. Ind. Eng. Chem.* **2019**, *70*, 264–275.
91. Deepa B, Rajendran V. Pure and Cu Metal Doped WO_3 Prepared via Co-Precipitation Method and Studies on Their Structural, Morphological, Electrochemical and Optical Properties. *Nano-Struct. Nano-Objects* **2018**, *16*, 185–192.
92. Hu P, Chen Y, Chen Y, Lin Z, Wang Z. Hydrothermal Synthesis and Photocatalytic Properties of WO_3 Nanorods by Using Capping Agent $SnCl_4 \cdot 5H_2O$. *Phys. E Low-Dimens. Syst. Nanostruct.* **2017**, *92*, 12–16.
93. Palharim PH, Caira MCDA, de Araújo Gusmão C, Ramos B, dos Santos GT, Rodrigues O, Jr., et al. Effect of Temperature and Time on the Hydrothermal Synthesis of WO3-AgCl Photocatalysts Regarding Photocatalytic Activity. *Chem. Eng. Res. Des.* **2022**, *188*, 935–953.
94. Yao S, Qu F, Wang G, Wu X. Facile Hydrothermal Synthesis of WO_3 Nanorods for Photocatalysts and Supercapacitors. *J. Alloys Compd.* **2017**, *724*, 695–702.
95. Mohamed MM, Salama TM, Hegazy MA, Abou Shahba RM, Mohamed SH. Synthesis of Hexagonal WO_3 Nanocrystals with Various Morphologies and Their Enhanced Electrocatalytic Activities toward Hydrogen Evolution. *Int. J. Hydrogen Energy* **2019**, *44*, 4724–4736.
96. Graham T. On the Properties of Silicic Acid and Other Analogous Colloidal Substances. *J. Chem. Soc.* **1864**, *17*, 318–327.
97. Parashar M, Shukla VK, Singh R. Metal Oxides Nanoparticles via Sol–Gel Method: A Review on Synthesis, Characterization and Applications. *J. Mater. Sci. Mater. Electron.* **2020**, *31*, 3729–3749.
98. Hench LL, West JK. The Sol-Gel Process. *Chem. Rev.* **1990**, *90*, 33–72.
99. Rezgui S, Gates BC. Sol-Gel Synthesis of Alumina in the Presence of Acetic Acid: Distinguishing Gels and Gelatinous Precipitates by NMR Spectroscopy. *Chem. Mater.* **1994**, *6*, 2386–2389.
100. Ciriminna R, Fidalgo A, Pandarus V, Béland F, Ilharco LM, Pagliaro M. The Sol–Gel Route to Advanced Silica-Based Materials and Recent Applications. *Chem. Rev.* **2013**, *113*, 6592–6620.
101. Tyagi B, Sidhpuria K, Shaik B, Jasra RV. Synthesis of Nanocrystalline Zirconia Using Sol−Gel and Precipitation Techniques. *Ind. Eng. Chem. Res.* **2006**, *45*, 8643–8650.
102. Nagarjuna R, Challagulla S, Sahu P, Roy S, Ganesan R. Polymerizable Sol–Gel Synthesis of Nano-Crystalline WO_3 and Its Photocatalytic Cr(VI) Reduction under Visible Light. *Adv. Powder Technol.* **2017**, *28*, 3265–3273.
103. Deganello F, Tyagi AK. Solution Combustion Synthesis, Energy and Environment: Best Parameters for Better Materials. *Prog. Cryst. Growth Charact. Mater.* **2018**, *64*, 23–61.
104. Varma A, Mukasyan AS, Rogachev AS, Manukyan KV. Solution Combustion Synthesis of Nanoscale Materials. *Chem. Rev.* **2016**, *116*, 14493–14586.
105. Chen P, Qin M, Chen Z, Jia B, Qu X. Solution Combustion Synthesis of Nanosized WOx: Characterization, Mechanism and Excellent Photocatalytic Properties. *RSC Adv.* **2016**, *6*, 83101–83109.
106. Zhang Y, Ding Y, Lan F, Zhang W, Li J, Zhang R. Recent Advances in Tungsten Oxide-Based Chromogenic Materials: Photochromism, Electrochromism, and Gasochromism. *Nanoscale* **2024**, *16*, 21279–21293.

107. Paik T, Cargnello M, Gordon TR, Zhang S, Yun H, Lee JD, et al. Photocatalytic Hydrogen Evolution from Substoichiometric Colloidal WO_{3-x} Nanowires. *ACS Energy Lett.* **2018**, *3*, 1904–1910.
108. Wang L, Tsang CS, Liu W, Zhang X, Zhang K, Ha E, et al. Disordered Layers on WO_3 Nanoparticles Enable Photochemical Generation of Hydrogen from Water. *J. Mater. Chem. A* **2019**, *7*, 221–227.
109. Zhang X, Hao W, Tsang CS, Liu M, Hwang GS, Lee LYS. Psesudocubic Phase Tungsten Oxide as a Photocatalyst for Hydrogen Evolution Reaction. *ACS Appl. Energy Mater.* **2019**, *2*, 8792–8800.
110. Yin M, Huang J, Zhu Z. Fabrication Novel WO_3@Cu Core-Shell Nanoparticles for High-Efficiency Hydrogen Generation under Visible Light by Photocatalytic Water Splitting. *Optik.* **2019**, *192*, 162938.
111. Toledo Camacho SY, Rey A, Hernández-Alonso MD, Llorca J, Medina F, Contreras S. Pd/TiO_2-WO_3 Photocatalysts for Hydrogen Generation from Water-Methanol Mixtures. *Appl. Surf. Sci.* **2018**, *455*, 570–580.
112. Pan L, Zhang J, Jia X, Ma YH, Zhang X, Wang L, et al. Highly Efficient Z-Scheme WO_{3-x} Quantum Dots/TiO2 for Photocatalytic Hydrogen Generation. *Chinese J. Catal.* **2017**, *38*, 253–259.
113. Jineesh P, Bhagya TC, Remya R, Shibli SMA. Photocatalytic Hydrogen Generation by WO3 in Synergism with Hematite-Anatase Heterojunction. *Int. J. Hydrogen Energy* **2020**, *45*, 18946–18960.
114. Tahir MB, Sagir M, Abas N. Enhanced Photocatalytic Performance of CdO-WO_3 Composite for Hydrogen Production. *Int. J. Hydrogen Energy* **2019**, *44*, 24690–24697.
115. Zhang LJ, Li S, Liu BK, Wang DJ, Xie TF. Highly Efficient CdS/WO_3 Photocatalysts: Z-Scheme Photocatalytic Mechanism for Their Enhanced Photocatalytic H_2 Evolution under Visible Light. *ACS Catal.* **2014**, *4*, 3724–3729.
116. Li F, Hou Y, Yu Z, Qian L, Sun L, Huang J, et al. Oxygen Deficiency Introduced to Z-Scheme CdS/WO_{3-x} Nanomaterials with MoS2 as the Cocatalyst towards Enhancing Visible-Light-Driven Hydrogen Evolution. *Nanoscale* **2019**, *11*, 10884–10895.
117. Hu T, Li P, Zhang J, Liang C, Dai K. Highly Efficient Direct Z-Scheme WO_3/CdS-Diethylenetriamine Photocatalyst and Its Enhanced Photocatalytic H_2 Evolution under Visible Light Irradiation. *Appl. Surf. Sci.* **2018**, *442*, 20–29.
118. Wang X, Maeda K, Thomas A, Takanabe K, Xin G, Carlsson JM, et al. A Metal-Free Polymeric Photocatalyst for Hydrogen Production from Water under Visible Light. *Nat. Mater.* **2009**, *8*, 76–80.
119. Cui L, Ding X, Wang Y, Shi H, Huang L, Zuo Y, et al. Facile Preparation of Z-Scheme WO_3/g-C_3N_4 Composite Photocatalyst with Enhanced Photocatalytic Performance under Visible Light. *Appl. Surf. Sci.* **2017**, *391*, 202–210.
120. Cheng C, Shi J, Hu Y, Guo L. WO_3/g-C_3N_4 Composites: One-Pot Preparation and Enhanced Photocatalytic H_2 Production under Visible-Light Irradiation. *Nanotechnology* **2017**, *28*, 164002.
121. Sun M, Zhou Y, Yu T, Wang J. Synthesis of G-C_3N_4/WO_3-Carbon Microsphere Composites for Photocatalytic Hydrogen Production. *Int. J. Hydrogen Energy* **2022**, *47*, 10261–10276.
122. Zhang L, Hao X, Li Y, Jin Z. Performance of WO_3/g-C_3N_4 Heterojunction Composite Boosting with NiS for Photocatalytic Hydrogen Evolution. *Appl. Surf. Sci.* **2020**, *499*, 143862.
123. Han X, Xu D, An L, Hou C, Li Y, Zhang Q, et al. WO_3/g-C_3N_4 Two-Dimensional Composites for Visible-Light Driven Photocatalytic Hydrogen Production. *Int. J. Hydrogen Energy* **2018**, *43*, 4845–4855.
124. Fu J, Xu Q, Low J, Jiang C, Yu J. Ultrathin 2D/2D WO_3/g-C_3N_4 Step-Scheme H2-Production Photocatalyst. *Appl. Catal. B Environ.* **2019**, *243*, 556–565.
125. Tahir MB, Nabi G, Khalid NR. Enhanced Photocatalytic Performance of Visible-Light Active Graphene-WO_3 Nanostructures for Hydrogen Production. *Mater. Sci. Semicond. Process.* **2018**, *84*, 36–41.
126. Alaoui C, Karmaoui M, Bekka A, Edelmannova MF, Gallardo JJ, Navas J, et al. TiO_2/WO_3/Graphene for Photocatalytic H2 Generation and Benzene Removal: Widely Employed Still an Ambiguous System. *J. Photochem. Photobiol. A Chem.* **2023**, *445*, 115020.
127. Ramírez-Ortega D, Guerrero-Araque D, Acevedo-Peña P, Lartundo-Rojas L, Zanella R. Effect of Pd and Cu Co-Catalyst on the Charge Carrier Trapping, Recombination and Transfer during Photocatalytic Hydrogen Evolution over WO_3-TiO_2 Heterojunction. *J. Mater. Sci.* **2020**, *55*, 16641–16658.
128. Zhao M, Liu S, Chen D, Zhang S, Carabineiro SAC, Lv K. A Novel S-Scheme 3D $ZnIn_2S_4$/WO_3 Heterostructure for Improved Hydrogen Production under Visible Light Irradiation. *Chinese J. Catal.* **2022**, *43*, 2615–2624.
129. Takagi M, Kawaguchi M, Yamakata A. Enhancement of UV-Responsive Photocatalysts Aided by Visible-Light Responsive Photocatalysts: Role of WO_3 for H_2 Evolution on CuCl. *Appl. Catal. B Environ.* **2020**, *263*, 118333.
130. Zhang M, Piao C, Wang D, Liu Z, Liu J, Zhang Z, et al. Fixed Z-Scheme TiO_2|Ti|WO_3 Composite Film as Recyclable and Reusable Photocatalyst for Highly Effective Hydrogen Production. *Opt. Mater.* **2020**, *99*, 109545.
131. Wang Y, Chen D, Hu Y, Qin L, Liang J, Sun X, et al. An Artificially Constructed Direct Z-Scheme Heterojunction: WO_3 Nanoparticle Decorated ZnIn2S4 for Efficient Photocatalytic Hydrogen Production. *Sustain. Energy Fuels* **2020**, *4*, 1681–1692.
132. Naseri N, Kim H, Choi W, Moshfegh AZ. Implementation of Ag Nanoparticle Incorporated WO_3 Thin Film Photoanode for Hydrogen Production. *Int. J. Hydrogen Energy* **2013**, *38*, 2117–2125.
133. Zhang L, Zhang H, Jiang C, Yuan J, Huang X, Liu P, et al. Z-Scheme System of WO3@MoS_2/CdS for Photocatalytic Evolution H_2: MoS_2 as the Charge Transfer Mode Switcher, Electron-Hole Mediator and Cocatalyst. *Appl. Catal. B Environ.* **2019**, *259*,

118073.
134. Wang D, Liu J, Zhang M, Song Y, Zhang Z, Wang J. Construction of Ternary Annular 2Z-Scheme+1Heterojunction CuO/WO_3/CdS/Photocatalytic System for Methylene Blue Degradation with Simultaneous Hydrogen Production. *Appl. Surf. Sci.* **2019**, *498*, 143843.
135. Li Z, Wang R, Wen M, Wang G, Xie G, Liu X, et al. WO_3/$Cd_{0.5}Zn_{0.5}S$ Heterojunction for Highly Efficient Visible-Light Photocatalytic H_2 Evolution. *J. Phys. Chem. Solids* **2023**, *178*, 111351.
136. Liu D, Zhang S, Wang J, Peng T, Li R. Direct Z-Scheme 2D/2D Photocatalyst Based on Ultrathin g-C_3N_4 and WO_3 Nanosheets for Efficient Visible-Light-Driven H_2 Generation. *ACS Appl. Mater. Interfaces* **2019**, *11*, 27913–27923.
137. Feng F, Hua H, Li L, Xu R, Tang J, Dong D, et al. Embedding 1D WO_3 Nanotubes into 2D Ultrathin Porous g-C_3N_4 to Improve the Stability and Efficiency of Photocatalytic Hydrogen Production. *ACS Appl. Energy Mater.* **2021**, *4*, 4365–4375.
138. Tahir MB, Rafique M, Isa Khan M, Majid A, Nazar F, Sagir M, et al. Enhanced Photocatalytic Hydrogen Energy Production of g-C_3N_4-WO_3 Composites under Visible Light Irradiation. *Int. J. Energy Res.* **2018**, *42*, 4667–4673.
139. Yan H, Liu YH, Yang Y, Zhang HY, Liu XR, Wei JZ, et al. Covalent Organic Framework Based WO_3@COF/RGO for Efficient Visible-Light-Driven H2 Evolution by Two-Step Separation Mode. *Chem. Eng. J.* **2022**, *431*, 133404.
140. Li Z, Jin D, Wang Z. $WO_3(H_2O)_{0.333}$/CdSe-Diethylenetriamine Nanocomposite as a Step-Scheme Photocatalyst for Hydrogen Production. *Surfaces and Interfaces* **2022**, *29*, 101702.
141. Oh WC, Na JD, Biswas MRUD. CVD Technique Assisted, Advanced Synthesis of WO_3-G Composites for Enhanced Photocatalytic H_2 Generation under Visible Light Illumination. *Fuller. Nanotub. Carbon Nanostruct.* **2019**, *27*, 762–769.
142. Wu K, Yao C, Wu P, Cao Y, Liu C, Chen P, et al. Highly Efficient Hydrogen Production Performance of g-C_3N_4 Quantum Dot-Sensitized WO_3/Ni–$ZnIn_2S_4$ Nanosheets. *Appl. Phys. A* **2022**, *128*, 903.
143. Zhou Y, Sun M, Yu T, Wang J. 3D g-C_3N_4/WO_3/Biochar/Cu^{2+}-Doped Carbon Spheres Composites: Synthesis and Visible-Light-Driven Photocatalytic Hydrogen Production. *Mater. Today Commun.* **2022**, *30*, 103084.
144. Shen R, Zhang L, Li N, Lou Z, Ma T, Zhang P, et al. W-N Bonds Precisely Boost Z-Scheme Interfacial Charge Transfer in g-C_3N_4/WO_3 Heterojunctions for Enhanced Photocatalytic H2 Evolution. *ACS Catal.* **2022**, *12*, 9994–10003.